Fermi National Accelerator Laboratory

FERMILAB-Pub-79/25-EXP
2085.000

HYPERON BEAM PHYSICS

J. Lach
Fermi National Accelerator Laboratory, Batavia, Illinois 60510

and

L. Pondrom
University of Wisconsin, Madison, Wisconsin

March 1979

(Reproduced by permission of Annual Reviews Inc. This article has been submitted for publication in Annual Review of Nuclear and Particle Science, Volume 29, to appear in December 1979)

HYPERON BEAM PHYSICS

J. Lach — Fermi National Accelerator Laboratory,[1] Batavia, Illinois 60510

L. Pondrom[2] — University of Wisconsin, Madison, Wisconsin 53706

[1] Operated by Universities Research Association Inc., under contract with the US Department of Energy.

[2] Supported in part by the US Department of Energy.

4. High Energy Hyperon Beams
    1. Introduction
    2. Fermilab Neutral Hyperon Beam
        1. Experimental Apparatus
        2. Inclusive Cross Sections
        3. A Dependence
        4. Polarization
        5. Magnetic Moments
        6. Elastic Scattering
    3. CERN SPS Charged Hyperon Beam
        1. Experimental Apparatus
        2. Hyperon Fluxes
        3. Ω^- Properties
    4. Fermilab Charged Hyperon Beam
5. Future Prospects

1 INTRODUCTION

Rochester and Butler (1947) first observed the decay of a neutral particle in a cloud chamber exposed to cosmic radiation. The mass of the neutral was at least 800 m_e, and represented a hitherto unknown phenomenon. Thus the age of strange particles began. Subsequent work by Armenteros et al (1951) showed that one neutral particle was heavier than the proton, with a quoted mass of $(2203 \pm 12)m_e$. In present notation this particle is a strange baryon, the Λ. Charged baryons in this mass range were also discovered. All of these particles exhibited the peculiar property that they were produced by strong interaction, yet decayed by weak interaction into strongly interacting particles. Thus the reaction $\pi^- p \xrightarrow[\text{strong}]{} \Lambda \xrightarrow[\text{weak}]{} \pi^- p$ is possible. To account for this effect a new quantum number called "strangeness" was introduced, which was assumed conserved by the strong and electromagnetic interactions. All ordinary strongly interacting particles were given S=0, whereas the new baryons, called hyperons, were given S=-1 and S=-2. This idea was proposed by Gell-Mann (1953). By the time of the review articles of Dalitz (1957) and Gell-Mann and Rosenfeld (1957) the classification scheme for the spin-parity $1/2^+$ hyperons, namely the Λ, an I-spin singlet with S=-1, the Σ^+, Σ^0, Σ^- an I-spin triplet also with

S=-1 and the Ξ^0, Ξ^- I-spin doublet with S=-2, was established in notation still in use at the present time. Table 1 shows the physical characteristics of these particles adopted and updated from the compilation of the Particle Data Group (1978).

The next step in classification of the hyperons was incorporation of I-spin and hypercharge Y = N + S, N being the baryon number, into the larger group SU_3. This procedure was proposed independently by Gell-Mann (1961) and Ne'eman (1961), and unified the six strange hyperons and the neutron and proton into an octet of $1/2^+$ baryons, shown schematically in Figure 1. The $3/2^+$ decuplet, in which only the most massive member, the Ω^-, has sufficiently long life to be observed in a hyperon beam, is also shown in the figure. The fundamental representations of the SU_3 group, from which the other representations can be formed, are triplets, called $\underline{3}$ and $\underline{3}^*$. The identification of the $\underline{3}$ with actual particles with remarkable properties was made, again independently, by Gell-Mann (1964) and Zweig (1964). Gell-Mann named the particles in the $\underline{3}$ representation quarks, and those in the $\underline{3}^*$ anti-quarks. The quark model of strange and non-strange hadrons constructs all of the particles from products of the form $\underline{3} \times \underline{3}^*$ for mesons and $\underline{3} \times \underline{3} \times \underline{3}$ for baryons. The number of quarks must be increased to

accommodate the newer charmed particles (Chinowsky 1977).

The SU_3 classification scheme incorporates over 100 hadronic states (both mesons and baryons) into multiplets, gives the mass splittings within each multiplet, and describes decay rates for those particles which decay by strong or electromagnetic interaction (Samios et al 1974). The group has also been used with success to relate strange baryon or meson total cross sections to their non-strange counterparts, and to predict properties of strange particle elastic and diffraction scattering off nucleons (Quigg and Rosner 1976).

There is a corresponding octet of antibaryons with the same masses and lifetimes but with opposite strangeness and hypercharge. They have all been observed, but only the antiproton has been extensively studied.

Application of SU_3 to the production of strange particles in hadronic collisions has not had such success because high energy particle production is not well understood, and it is difficult to separate phenomena which might be related by group theory from other effects. A reaction of the type $p + p \rightarrow A + X$, where X is not observed is called an "inclusive" reaction, reviewed by Boggild and Ferbel (1974). The invariant cross section $Ed^3\sigma/dp^3$ is usually written as either a function of $(x, p_\perp)$ or

$(y,p_\perp)$, where $x = p^*_{\parallel}/p^*_{\parallel max}$, $y = 1/2\ \ln((E+p^*_{\parallel})/(E-p^*_{\parallel}))$, $p^*_{\parallel}$ = longitudinal momentum, and $p_\perp$ = transverse momentum of the produced particle in the center of mass. Strange baryons are produced about 10% of the time in p-p collisions, and all final state baryons exhibit the "leading particle effect" to some degree. If a baryon is incident in the initial state, baryons occurring in the final state are enhanced relative to mesons. The hyperons Λ, $\Sigma^{\pm}$, Σ° show this effect quite distinctly as $x \to 1$, while the enhancement of Ξ^- and Ξ° is less marked. The production of antihyperons in pp collisions resembles anti-proton production and has no leading particle effect at all. This leading particle enhancement has important practicle consequences in the design of hyperon beams.

As shown in Table I the hyperons, with the exception of the Σ°, all have lifetimes in the 10^{-10} sec range. They all predominantly decay non-leptonically into pion-nucleon for Λ, $\Sigma^{\pm}$, into pion-Λ for Ξ, and into ΛK^- or $\Xi\pi$ for the Ω^-. The properties of the non-leptonic decays

Table 1

Properties of the Hyperons[a]

Spin-parity $1/2^+$

Name	Mass MeV/c^2	Lifetime Sec	Decay Length cm/GeV/c	Magnetic Moment $e\hbar/2m_pc$
Λ	1115.60±.05	$(2.632\pm.020)\times10^{-10}$	6.93	$-0.6138\pm.0047$[b]
Σ^+	1189.37±.06	$(0.802\pm.005)\times10^{-10}$	2.02	2.95± .31
Σ°	1192.47±.08	$(.58\pm.13)\times10^{-19}$	——	——
Σ^-	1197.35±.06	$(1.483\pm.015)\times10^{-10}$	3.71	-1.48 ± .37
Ξ°	1314.9 ±.6	$(2.90\pm.10)\times10^{-10}$	6.59	-1.20 ± .06[c]
Ξ^-	1321.32±.13	$(1.654\pm.021)\times10^{-10}$	3.75	-1.85 ± .75
		spin-parity $3/2^+$		
Ω^-	1672.2 ±.4	$(.82\pm.06)\times10^{-10}$[d]	1.47	——

a.) Particle Data Group (1978) except as otherwise noted

b.) Schachinger et al (1978)

c.) Bunce et al (1979)

d.) Bourquin et al (1978)

are shown in Table 2. In each non-leptonic decay the I-spin of the final state must differ from the I-spin of the initial state by 1/2 integer. Amplitudes for which $|\Delta\vec{I}| = 1/2$ seem to dominate. The phenomenological description of the parameters of the decays, and the sensitivity to various symmetry tests have been reviewed by Overseth and Pakvasa (1969). The experimental situation is periodically reviewed by Overseth as a part of the Particle Data Group report (1978). The non-leptonic two-body decay is often used in a hyperon beam to detect the presence of the parent hyperon. In this case the α parameters, listed in Table 2, are of especial importance, because $\alpha \neq 0$ leads to an asymmetrical distribution of decay products if the hyperons are polarized. In the general case a $J = 1/2 \rightarrow J = 1/2$ transition without parity conservation can involve both an $\ell = 0$ amplitude, S, and an $\ell = 1$ amplitude P. The three components of the final state baryon polarization are described in terms of constants α, β, and γ where $\alpha = 2\,\mathrm{Re}S^*P/(|S|^2 + |P|^2)$, $\beta = 2\,\mathrm{Im}\,S^*P/(|S|^2 + |P|^2)$, and $\gamma = (|S|^2 - |P|^2)/(|S|^2 + |P|^2)$. If the parent hyperon has polarization $\vec{P}_Y$, the final state baryon distribution is of the form $(1 + \alpha \vec{P}_Y \cdot \hat{k})$, where $\hat{k}$ is the

Table 2

Non-Leptonic Decays[a]

Particle	Mode	Branding Ratio[b]	Decay Parameters[c] α	ϕ
Λ	$p\pi^-$	(64.2 ±.5)%	+.647±.013	(-6.5±3.5)°
Λ	$n\pi^\circ$	(35.8 ±.5)%	+.646±.044	——
Σ^+	$p\pi^\circ$	(51.6 ±.7)%	-.979±.016	(36 ± 34)°
Σ^+	$n\pi^+$	(48.4 ±.7)%	+.072±.015	(167 ± 20)°
Σ°	$\Lambda\gamma$	100%	————	
Σ^-	$n\pi^-$	100%	-.069±.008	(10 ± 15)°
Ξ°	$\Lambda\,\pi^\circ$	100%	-.478±.035[e]	(21 ± 12)°
Ξ^-	$\Lambda\,\pi^-$	100%	-.392±.021	(2 ± 6)°
Ω^-	$\Lambda\,K^-$	(67.0±2.2)%[f]	.06 ±.14[f]	
Ω^-	$\Xi^\circ\pi^-$	(2.46±1.9)%[f]	————	
Ω^-	$\Xi^-\pi^\circ$	(8.4 ±1.1)%[f]	————	

a.) Particle Data Group (1978)

b.) Ignores rare modes (see Table 3)

c.) α is the final state baryon helicity. The decay parameters β and γ are defined by $\beta = \sqrt{1-\alpha^2}\sin\phi$, $\gamma = \sqrt{1-\alpha^2}\cos\phi$. See text.

d.) The Σ° decays mainly by electromagnetic interaction.

e.) Bunce et al (1978)

f.) Bourquin et al (1978)

momentum unit vector of the final state baryon in the hyperon rest frame. Alternatively if the parent hyperon is unpolarized, the final state baryon is longitudinally polarized with $\langle \vec{P} \rangle = \alpha \hat{k}$. The polarization of the final state baryon in the general case also involves the parameters β and γ multiplied by P_γ.

Table 3 shows the branching ratios and decay parameters for the rarer semi-leptonic decays of the hyperons. For many of the semi-leptonic final states only the branching ratio is known, and that with large uncertainty. The ratio g_A/g_V given in the Table for $\Lambda \rightarrow pe^-\bar{\nu}_e$, $\Sigma^- \rightarrow ne^-\bar{\nu}_e$ and $\Sigma^- \rightarrow \Lambda e^-\bar{\nu}_e$ represents the axial vector to vector coupling constant. The determination of this coupling constant ratio requires a measurement of the momentum correlation of the hyperon decay products. Cabibbo (1963) proposed a model, based on SU_3, which unifies the semi-leptonic decays of strange and non-strange baryons. The present data are consistent with this model (Tanenbaum et al 1975). A more detailed discussion of these decays will be given below.

Table 3

Semi Leptonic Decays[a]

Particle	Mode	Branching	g_A/g_V	g_V/g_A
Λ°	$pe^-\bar{\nu}_e$	$(8.13\pm.29)\times10^{-4}$	$-.62\pm.05$	
	$p\mu^-\bar{\nu}_\mu$	$(1.57\pm.35)\times10^{-4}$	—	
Σ^+	$Ae^+\nu_e$	$(2.02\pm.47)\times10^{-5}$	—	
	$ne^+\nu_e$	$.5\times10^{-5}$	—	
Σ^-	$ne^-\bar{\nu}_e$	$(1.08\pm.04)\times10^{-3}$	$.385\pm.070$	
	$n\mu^-\bar{\nu}_\mu$	$(.45\pm.04)\times10^{-3}$	—	
	$Ae^-\bar{\nu}e$	$(.60\pm.06)\times10^{-4}$		$.24\pm.23$
Ξ°	$\Sigma^+e^-\bar{\nu}_e$	$<1.1\times10^{-3}$[b]		
Ξ^-	$Ae^-\bar{\nu}_e$	$(.69\pm.18)\times10^{-3}$		
Ω^-	$Ae^-\bar{\nu}_e$	$\sim10^{-2}$[c]		

a.) Particle Data Group (1978)

b.) Only upper limits exist for the semi-leptonic channels of the Ξ°.

c.) Bourguin et al (1978).

2 HYPERON BEAM CONSTRUCTION

The term hyperon beam refers to a secondary beam of particles, usually produced by striking a metal or refractory target with the primary proton beam of an accelerator, which is collimated to a reasonably small solid angle, and which contains a useful flux of hyperons together with a background of the more copiously produced particles. If the beam is negatively charged, pions are the largest background. If it is positively charged, then usually protons are most numerous. In a neutral beam both neutrons and γ rays are present in numbers exceeding the flux of hyperons. Charged beams can be deflected by dipole magnets and focused by quadrupoles like any other secondary beam. In general, a hyperon beam supplies a high flux of short-lived particles which can be used to study their decays and their interactions with ordinary matter in a manner similar to the one traditionally employed for the more common longer lived particles.

The fourth column of Table 1 illustrates a central design problem, for it gives constants which, when multiplied by the hyperon momentum in GeV/c, give the decay lengths of the particles in cm in the laboratory. For example, a 10 GeV/c Λ beam is attenuated by 1/e in

only 69 cm. Since the fractional yield of hyperons at the target remains essentially constant at about 10% as the energy is increased, good hyperon beams clearly become easier to make at higher energy, provided that the length necessary to shield the experiment from the primary production target does not also scale with the energy. This is indeed the case, because adequate shielding for hadronic cascade requires a thickness of material which grows only logarithmically with the primary energy. Thus, as will be seen below, beam lines designed to operate at 400 GeV are only about a factor of two longer than those designed for 30 GeV, which gives a substantial advantage in signal-to-noise to the higher energy beams.

3 FIRST GENERATION HYPERON BEAMS

3.1 Introduction

Although hyperons had been observed earlier in short neutral beams designed for study of K_S° - K_L° complex (Jensen et al 1969), it was not until the late 1960's that special effort was placed on the design of charged and neutral beams specifically for hyperon studies. Two companion beams were constructed nearly simultaneously for charged hyperons, one at the CERN PS and the other at the Brookhaven AGS. A preview of these beams

before their operation was given by Sandweiss (1971). In addition, a short neutral beam for Λ and Ξ^0 hyperons was built at the CERN PS. A similar neutral beam was subsequently built at Brookhaven.

Table 4 summarizes the operational characteristics of these beams. The Brookhaven AGS charged beam layout is shown in Figure 2 (Hungerbuhler et al 1974a); the corresponding CERN charged beam layout is shown in Figure 3 (Badier et al 1972a). The design of both these beams was shaped by two requirements; first that the beam be as compact as possible to reduce hyperon decay losses. This meant that a premium was set on high magnetic fields and high spatial resolution detectors used to determine the hyperon trajectories. The second goal was to interact the secondary hadrons produced outside of the beam phase space as far upstream in the beam as practical; before they could decay to muons or generate other backgrounds nearer the experimental apparatus. Care was taken to make the coils of the dipole magnets sufficiently large so that those muons produced in the target region and deflected away from the experimental apparatus by the central magnetic field were not redirected into the apparatus when they passed

through the coils into the return flux region. Since the actual hyperon channel region was only a few square centimeters in cross section high magnetic fields ($\sim$ 32kG) could be achieved by shimming standard dipole magnets.

In the Brookhaven beam the hyperons were detected by their decay immediately after a high resolution (σ = 100 μm), high pressure spark chamber (Willis et al, 1971). This counter allowed the hyperon trajectory to be reconstructed and extrapolated back to the production target as a verification of its origin and also served to measure its momentum. The pion background was suppressed by a threshold gas Cerenkov counter in the downstream end of the magnetic channel and used to tag particles with $m \leq m_p$.

Table 4

Characteristics of Hyperon Beams

Location[a]	E GeV	I_p per pulse	TGT	Θ mrad	E_Y GeV	L m	I_Y per pulse	I_{TOT}
AGS[b] charged	29	1.5×10^{11}	Be	0	17-26	4.4	$200\Sigma^-$ $2\Sigma^-$	30,000 π^-
PS[c] charged	24	10^{11}	B_4C W Al	10	13-20	3	50 Σ^- 1 Ξ^-	25,000 π^-
Ps[d] neutral	24	10^9	Pt	175	3-15[e]	2	500 Λ	100,000 n
AGS[f]	30	10^{9g}	Ir	72	8-16	2	500 Λ	h
FNAL[i] neutral	400	10^8	Cu Be Pb	0-10	70-350	6	5,000	200,000 n 400,000 γ
SPS[j] charged	200	4×10^{10}	BeO	2^- 6^+	70-140	12	4,000Σ^-_+ 46 Σ^+	$10^6\pi^-$ 10^6p

Table 4

(continued)

a.) Column headings are: E_p, I_p = primary beam energy and intensity; TGT, θ = production target and angle; E_Y = hyperon beam energy; L = magnetic channel length; I_Y, I_{TOT} = typical hyperon and total fluxes.

b.) Data from Hungerbuhler et al (1974b and 1975).

c.) Data from Badier et al (1972a).

d.) Data from Geweniger et al (1974).

e.) For a neutral beam, this is the approximate energy spread after the magnetic channel.

f.) Private communication from D. Jensen (1978).

g.) Proton maximum flux capability 2×10^{11}.

h.) γ rays selectively removed by $10X_{rad}$ of lead at entrance to collimator.

i.) Data from Skubic, et al (1978).

j.) Data from Bourguin, et al (1979).

The CERN beam embodied a set of superconducting quadrupole magnets in the hyperon channel which produced a parallel beam and allowed the use of a DISC Cerenkov counter for particle identification. The performance of these high resolution differential gas Cerenkov counters has been described by Litt & Meunier (1973). A pressure scan with the DISC counter showed clearly resolved peaks corresponding to Σ^- and Ξ^- as well the more copious other hadrons. Both beams had useable fluxes of negative hyperons with tolerable backgrounds of pions in the beam and of general background radiation - mostly muons which were not stopped in the shielding. It was not found practical to use the Σ^+ beam because of the shorter decay length of the hyperons and the high flux of protons. Each group undertook an experimental program to: a.) study hyperon production yields; b.) measure hyperon interaction cross sections; c.) investigate the various hyperon decay modes.

3.2 Hyperon Production Cross Sections

Badier et al (1972a) obtained ratios Σ^-/π^- and Ξ^-/π^- for various production angles, secondary beam momenta, and targets by comparing the areas under the peaks of their DISC curves and making suitable corrections for hyperon decays between the production target and the DISC. Their hyperon cross sections are then obtained by using the normalized π^- inclusive cross sections of Eichten et al (1972).

Hungerbuhler et al (1975) also measured ratios Σ^-/π^- and Ξ^-/π^- by detecting the decays $\Sigma^- \rightarrow n\pi^-$ and $\Xi^- \rightarrow \Lambda\,\pi^-$ in the downstream spectrometer shown in Figure 2. These ratios could be extrapolated back to the hyperon production target by correcting them for detection losses and hyperon decays in the magnetic channel. Invariant inclusive cross sections $Ed^3\sigma/dp^3$ for Σ^- and Ξ^- production on beryllium at 0 mrad production angle and various secondary momenta between 17 and 26 GeV/c were then obtained by using the π^- invariant cross sections given by the empirical fit of Wang (1970). The Wang fit does not reproduce π^- production measurements (Allaby et al 1970) well near the kinematic limit. Hence this group used the Wang fit only in the region away from the kinematic

limit where it is in good agreement with data. A target interaction monitor and the known scaling properties of the hyperon magnetic channel with momentum allowed them to compute the hyperon invariant cross section in the full momentum range of their measurements.

Figure 4 shows a comparison of the hyperon invariant cross section measurements as a function of x of Hungerbuhler et al (1975) at 0 mrad and those of Badier et al (1972a) at 10 mrad. The data of Badier et al have been converted from a tungsten target to a beryllium target by using the measured A dependence from Table 2 of their paper. Cross sections for the more common particles at 12.5 mrad are also shown in the figure from the work of Allaby et al (1970). Because of uncertainties in the angle dependence of the cross sections, no attempt was made to convert the various experiments to the same production angle. Care was taken to compute x in a manner consistent with conservation of charge, baryon number, and strangeness, because differences in the maximum allowed longitudinal momenta, although small, are not negligible at these energies. Some ambiguity in p_{max} remains due to Fermi motion in the complex nucleus

and whether a neutron or a proton was the target. It is interesting to note that above $x \gtrsim 0.75$ the Σ^- cross section exceeds the π^- cross section, demonstrating the leading particle effect. The Σ^- yield is roughly 1% of the proton yield. The Ξ^- cross section drops off more rapidly with increasing α, more like $\bar{p}$'s and is smaller than the Σ^- by a factor of about 1/25 at $x = 0.7$.

3.3 Hyperon Interaction Cross Sections

3.3.1 Introduction

These companion negative hyperon beams had sufficient flux to permit practical measurements of various hyperon interaction cross sections in a more or less conventional fashion, thus achieving a considerable improvement in precision over previous work, where hyperon interactions were studied in bubble chambers.

The two original charged hyperon groups studied Σ^- interactions in hydrogen; the CERN group also used deuterium. At CERN Badier et al (1972b) measured the Σ^-p and Σ^-d total cross sections, and Blaising et al (1975) and Blaising (1977) measured Σ^-p elastic

scattering, all with cryogenic targets. At Brookhaven Majka et al (1976) and Majka (1974) studied $\Sigma^- p$ and $\Xi^- p$ elastic scattering with a liquid hydrogen target. The same group Hungerbuhler et al (1974) and Hungerbuhler (1973) studied Σ^- and Ξ^- interactions in a plastic scintillator target. Subsequently Arik et al (1977) and Arik (1976) studied Y* production in Σ^- nucleus reactions with the Brookhaven charged hyperon beam on hydrogen, aluminum, copper, tungsten, and lead targets. The CERN neutral hyperon beam, listed in Table 4 but not yet described, also played an important role in hyperon interaction studies. Gjesdal et al (1972) obtained Λp, $\bar{\Lambda} p$, Λd, $\bar{\Lambda} d$ total cross sections by CH_2 - C or D_2O - H_2O subtraction, and Dydak et al (1977) measured the Σ° lifetime by studying the process $\Lambda + \gamma \rightarrow \Sigma^\circ$, where the "$\gamma$ ray" was supplied by the Coulomb field of a heavy nucleus.

The SU_3 quark model predicts differences between strange and ordinary particle total cross sections on a given target. The relation between hydrogen total cross sections

$$\sigma_T (\Lambda p) - \sigma_T (pp) = \sigma_T (K^- n) - \sigma_T (\pi^+ p) \quad (1)$$

was first written down by Lipkin & Scheck (1966) using

simple quark counting rules to decompose the amplitude, and then the optical theorem to relate the forward amplitude to the total cross section. Other relations of this type are

$$\sigma_T(pp) - \sigma_T(\Sigma^- p) = \sigma_T(\pi^- p) - \sigma_T(K^- p) + 2[\sigma_T(K^+ p) - \sigma_T(K^+ n)], \quad (2)$$

$$\sigma_T(pp) - \sigma_T(\Sigma^- n) = \sigma_T(\pi^- p) - \sigma_T(K^- p), \quad (3)$$

$$\sigma_T(pd) - \sigma_T(\Sigma^- d) = \sigma_T(\pi^- d) - \sigma_T(K^- d), \quad (4)$$

and

$$\sigma_T(\Sigma^- p) + \sigma_T(\Sigma^- n) = 2\sigma_T(\Lambda p). \quad (5)$$

The pertinent nucleon-nucleon, pion-nucleon, and kaon-nucleon cross section data needed to predict the hyperon cross sections via these equations is supplied in the review article by Giacomelli (1976).

Giacomelli (1976) also discusses differential elastic scattering at high energies throughout the complete range of momentum transfers. High energy differential elastic cross sections are written $d\sigma/d|t|$, in units $mb/(GeV/c)^2$, where the variable t is the 4-momentum transfer. In the elastic process $a + b \rightarrow a + b$, the variables commonly used are $s = -(P_a + P_b)^2$, $t = -(P_a - P_a')^2$, $u = -(P_a - P_b')^2$, where P_a is a 4-vector

with metric $P_a \cdot P_a = -m_a^2$, the prime denotes the final state, and $s + t + u = 2(m_a^2 + m_b^2)$. For particle a incident on target b at rest, s, which is the square of the total available energy, is given by $s = m_a^2 + m_b^2 + 2m_b E_a$, and $t = 2m_a^2 - 2 E_a E_a' + 2\vec{p}_a \cdot \vec{p}_a'$. In terms of the laboratory kinetic energy of the recoiling target particle, the variable $t = -2m_b(E_b' - m_b) = -2m_b T_b'$. The experimental cross section $d\sigma/d|t|$ is often empirically fit by an exponential of the form

$$\frac{d\sigma}{d|t|} = A \exp(bt + ct^2). \qquad (6)$$

For small $|t|$, the cross section is approximately exponential in $|t|$ with slope parameter b. By convention, an effective slope parameter at $|t| = 0.2(\text{GeV/c})^2$ is often used to compare various experiments. At $|t| = 0$, $d\sigma/d|t| = A$, which is called the optical point. If it is assumed that the forward amplitude is predominantly imaginary, it is directly related to the total cross section through the optical theorem, so that

$$A(\text{mb}/(\text{GeV/c})^2) = 5.095 \times 10^{-2} (\sigma_T(\text{mb}))^2.$$

A very simple geometrical picture of high energy small $|t|$ diffraction scattering relates the slope parameter b and the total cross section to the radius R of the disc: $\sigma_T \sim R^2$, $b \sim R^2$, or $\sigma_T/b = \text{constant}$. Thus larger

total cross sections lead to steeper elastic scattering slopes in this model. The logarithmic growth with energy of σ_T is interpreted as a change in the radius of the disc. These concepts are useful in discussing hyperon elastic scattering.

3.3.2 Total Cross Section Measurements

The high resolution DISC Cerenkov counter was the hyperon detector for Badier et al (1972b) in their total cross section measurements. Two such counters were used, one on either side of a cryogenic hydrogen (H) or deuterium (D) target. A vacuum target (V) was used to correct for absorption in the target walls. Multiwire proportional chambers on either end of the DISC's measured the trajectory of the hyperon before and after the hydrogen target, while the Cerenkov light in the DISC's identified hyperons in the presence of the pion background. The angular acceptance of the second DISC was made large ($\pm$ 12 mrad compared to $\pm$ 5 mrad for DISC 1) to accept diffractively scattered Σ^-'s as well as beam Σ^-. The beam was tuned to 18.7 GeV/c. The number of Σ's scattered through angles $\theta < \theta_{max}$ per incident beam Σ was measured for each of the three targets H, D, V. To obtain the correct total cross

sections $\sigma_T(\Sigma^- p)$ and $\sigma_T(\Sigma^- d)$ as $\theta_{max} \to 0$ it was necessary to take multiple coulomb scattering into account, and to add the forward elastic $\Sigma^- p$ or $\Sigma^- d$ nuclear scattering contribution, while subtracting the contributions from coulomb single scattering and nuclear-coulomb interference. The difference $\sigma_T(\Sigma^- d) - \sigma_T(\Sigma^- p) = \sigma_T(\Sigma^- n) - \delta$, where δ corrects for screening of one nucleon by the other. The theory of this effect has been worked out by Glauber (1960) and Harrington (1964). Badier et al (1972b) obtained the following cross sections at 18.7 GeV/c:

$$\sigma_T(\Sigma^- p) = 34.0 \pm 1.1 \text{ mb} \quad (7)$$

$$\sigma_T(\Sigma^- d) = 61.3 \pm 1.4 \text{ mb} \quad (8)$$

$$\sigma_T(\Sigma^- n) = 30.0 \pm 1.8 \text{ mb} \quad (9)$$

The short neutral beam constructed at the CERN PS and described by Geweniger et al (1974) was designed to measure Λ and $\bar{\Lambda}$ total cross sections by CH_2 - C or D_2O - H_2O subtraction. The absorption of neutral hyperons in the two targets was measured at the same time to eliminate systematic errors due to intensity fluctuations by splitting the target transverse to the beam. Downstream of this target arrangement the decays $\Lambda \to p\pi^-$ and $\bar{\Lambda} \to \bar{p}\pi^+$ were detected in a multiwire proportional

chamber magnetic spectrometer. Their apparatus, configured for a different experiment, is shown in Figure 5. Gjesdal et al (1972) note that, although the simultaneous transmission method eliminates many troubles in obtaining the total cross section, care had to be taken to insure that the decays observed were really $\Lambda \rightarrow p\pi^-$ and $\bar{\Lambda} \rightarrow \bar{p}\,\pi^+$, that it was clear which half of the target the hyperon traversed, and that those hyperons which either scattered in the target or were produced there by beam neutrons be eliminated from the transmitted hyperon flux. Cross sections were obtained as a function of hyperon momentum in 15 bins between 6 GeV/c and 21 GeV/c. Observing no significant variation in cross section with momentum, the authors quote the following average values:

$$6 \text{ GeV/c} \leq p_\Lambda \leq 21 \text{ GeV/c}$$

$$\sigma_T(\Lambda p) = 34.6 \pm 0.4 \text{ mb} \qquad (10)$$

$$\sigma_T(\Lambda d) - \sigma_T(\Lambda p) = 31.2 \pm 0.7 \text{ mb} \qquad (11)$$

$$\sigma_T(\Lambda n) = 34.0 \pm 0.8 \text{ mb} \qquad (12)$$

where Equation (12) was obtained from Equation (11) by applying the screening correction discussed above. For $\bar{\Lambda}$ with an average momentum of $p_{\bar{\Lambda}} = (9.2 \pm 2.0)$ GeV/c, they obtained $\sigma_T(\bar{\Lambda}p) = (56 \pm 11)$ mb and $\sigma_T(\bar{\Lambda}n) = 46 \pm 20)$ mb.

Equation (1) can be solved for $\sigma_T(\Lambda p)$, giving the prediction $\sigma_T(\Lambda p) = (35.2\pm0.6)$ mb in this energy range. The difference σ(predicted) - σ(measured) = (0.6±0.7) mb, in good agreement with the simple quark model. The equality of Λp and Λn cross sections is expected from charge symmetry, since the Λ has I-spin zero. Using the charged hyperon results of Equations (7) and (9), together with Equation (5), $\sigma_T(\Lambda p) = (32.0\pm1.1)$ mb. Here the difference σ(predicted) - σ(measured) = (-2.6±1.2) mb, which is not in such good agreement with the quark model. The problem is that the measured $\Sigma^- n$ cross section, Equation (9), is too small. Equation (2) predicts $\sigma_T(\Sigma^- p) = (35.0\pm0.9)$ mb, in good agreement with Equation (7), whereas Equation (3) predicts $\sigma_T(\Sigma^- n) = (38.5\pm0.8)$ mb, about 4 standard deviations larger than the experimental result in Equation (9).

3.3.3 Scattering Cross Section Measurements

It is helpful to detect the recoil proton as a signature for $\Sigma^- p$ elastic scattering, and both the CERN experiment of Blaising et al (1975) and the Brookhaven experiment of Majka et al (1976) did this. Since a proton of $T_p \leq 50$ MeV does not have sufficient range to leave the target vessel, a practical lower limit was placed on $|t| \geq 0.1$.

The CERN experiment covered the range $0.2 \leq |t| \leq 0.38$ GeV/c^2 at 17.2 GeV/c incident Σ^-, and collected 2826 Σ^-p elastic events. The Brookhaven experiment covered the range $0.1 \leq |t| \leq 0.23$ (GeV/c)^2 at 23 GeV/c incident Σ^-, and collected 6200 Σ^-p elastic events. They also obtained 67 Ξ^-p events in the same data sample. Since negative pions were copiously supplied by both beams, it was convenient to measure the π^-p cross section as well, which was already well known in this $|t|$ range from other experiments. The CERN group normalized their Σ^-p relative to π^-p. The Brookhaven group normalized both cross sections absolutely, and used their π^-p result as a check on the over-all technique.

Figure 6 shows the results of these two experiments. The fit of the Σ^- data to the form of Equation 6, shown in Figure 7, did not require a t^2 term in the exponent. The results are summarized in Table 5. The slopes agree with each other, and are in good agreement with the

Table 5

$\Sigma^- p$ Elastic Scattering

$d\sigma/d|t| = Ae^{bt}$

Expt	p_Σ GeV/c	$\|t\|$ range $(GeV/c)^2$	b $(GeV/c)^{-2}$	A_{meas} $mb/(GeV/c)^2$	A^b_{opt} $mb/(GeV/c)^2$
BNL[a]	23	0.1-0.23	8.99±0.39	30±3	59±3
CERN[c]	17.2	0.12-0.38	8.12±0.35	47.4±4.9	59±3

a.) Majka et al (1976)

b.) Derived from σ_T = (34±1) mb of Badier et al (1972b)

c.) Blaising et al (1975)

prediction of the disc diffraction model: $b_{\Sigma^- p} = b_{pp}$ $\sigma_T(\Sigma^- p)/\sigma_T(pp)$, which gives $b_{\Sigma^- p}$ = 8.7±0.5 $(GeV/c)^{-2}$. The over all normalizations of the two experiments disagree by three standard deviations, assuming that the elastic cross section changes a negligible amount between 17 and 23 GeV. Both extrapolations to t = 0 are below the optical point, the Brookhaven result being (29±4) mb low. A careful measurement of the low $|t|$ region in high energy pp elastic scattering by Barbiellini et al (1972) showed that the slope parameter below $|t| \lesssim 0.1$ $(GeV/c)^2$ was distinctly larger than above that $|t|$ value by about 1.5 to 2.0 $(GeV/c)^{-2}$. This slope change at small $|t|$appears to be a general phenomenon in hadron elastic scattering and has been noticed par-

ticularly by experiments performed in the Coulomb-nuclear interference region (Lach 1976). A recent summary of pp and $\pi^- p$ slope changes as a function of t is given by Burq et al (1978). A slope change of this magnitude increases the cross section extrapolated to t=0 by about 15%, bringing the CERN result up to 54 mb, and the Brookhaven result to 35 mb; the agreement is still poor.

3.3.4 Σ° Lifetime

Dydak et al (1977) measured the lifetime of the Σ° hyperon in a remarkable experiment in the CERN neutral hyperon beam. The decay rate $\Gamma(\Sigma^\circ \to \Lambda\gamma)$ should be proportional to the square of the transition magnetic moment $\mu_{\Sigma\Lambda}$ which was predicted from SU_3 by Coleman and Glashow (1961). The expected Σ° lifetime based on these considerations is $\tau_{\Sigma^\circ} = 0.7 \times 10^{-19}$ sec, corresponding to a flight path of 0.2 $\mathring{A}$ per GeV/c momentum, or a mass width $\Delta m = 9.4$ keV. Neither the flight distance nor the mass width can be measured by present day techniques. The decay rate can be measured indirectly by studying the reaction $\Lambda + Z \to \Sigma^\circ + Z$, where the coulomb field of the nucleus Z supplies the "γ" for the inverse process $\Lambda + \gamma \to \Sigma^\circ$. This mechanism, called the Primakoff effect,

has been discussed in detail by Dreitlein and Primakoff (1962). The cross section is proportional to Z^2/τ_{Σ^0}; it is sharply peaked in the forward direction within an angle of about 2 mrad for 10 GeV/c Λ's; and it increases logarithmically with increasing energy. Competting strong interactions which convert Λ's into Σ^0's do not have these characteristics.

The experimental procedure then was to insert a thin high Z target in the neutral beam (U and Ni were used); to look for $\Lambda\ \gamma$ downstream of the target by detecting the decay $\Lambda \rightarrow p\pi^-$ and converting the γ-ray. A very sharp peak was expected for $(\Lambda\gamma)$ events with invariant mass $m_{\Lambda\gamma} \approx m_{\Sigma}$ at very small angles relative to the (unobserved) incident beam Λ. The apparatus used by Dydak et al to do this is shown in Figure 5. The $\Lambda \rightarrow p\pi^-$ was measured in their multiwire proportional chamber spectrometer, and the γ ray energy and location was recorded in an array of 84 lead glass blocks each 12.7 radiation lengths deep. The $\Lambda \rightarrow p\pi^-$ mass resolution had a $\sigma = 1.5\ MeV/c^2$. The energy resolution of the lead glass was $\Delta E/E = 0.11/\sqrt{E(GeV)}$ full width at half maximum, and by calculating the centroid of the electromagnetic shower energy they obtained a position resolution $\sigma = 2.7$ cm. The reconstructed Λ momentum vector intersected the plane of

the Primakoff target at a point P, giving the origin of the Σ^0. A line between P and the production target center gave the incident Λ line of flight to within σ = 1.2 mrad.

The uranium data for those $\Lambda\gamma$ events with mass $1.175 \leq m(\Lambda\gamma) \leq 1.205$ GeV/c^2 is shown in Figure 7 plotted as a function of $q^2 = p_\Sigma{}^2\theta_\Sigma^2$. The background was predominantly due to decays of beam Ξ^0's, $\Xi^0 \rightarrow \Lambda\pi^0$, where only one γ ray from the decay $\pi^0 \rightarrow \gamma\gamma$ was detected by the lead glass. The peak at small q^2, was ascribed entirely to the Primakoff effect. Analysis of these data and similar results from nickel gave a lifetime $\tau_{\Sigma^0} = (0.62 \pm 0.10 \times 10^{-19}$ sec, in good agreement with the SU_3 prediction.

3.4 RARE DECAYS

3.4.1 Description of Semileptonic Decays

Hyperon beta decays are very difficult to study. The branching ratios, given in column 3 of Table 3, are all small. In addition, two neutral particles are always involved, a neutrino and a neutral baryon. If the parent baryon is a Λ, or the daughter is a neutron, usually only the baryon direction is measured, not its energy. Thus a process like $\Sigma^- \rightarrow ne^-\bar{\nu}_e$ or $\Lambda \rightarrow pe^-\bar{\nu}_e$ has a zero constraint kinematic fit. Decays like $\Sigma \rightarrow \Lambda e^-\bar{\nu}_e$, or $\Xi^- \rightarrow \Lambda e^-\bar{\nu}_e$, where $\Lambda \rightarrow p\pi^-$ can be observed in the final

state, pick up a helpful extra constraint. The decay asymmetry allows the final state baryon spin direction to be measured as well. But for the other decays the zero constraint fit leads to a quadratic ambiguity and two solutions for the energy of the neutral baryon. Low rates and weak kinematic constraints make it difficult to accumulate many events, and make the data sample prone to contamination by background, which is often composed of mis-identified non-leptonic decays of the same hyperons.

The semi leptonic decays are especially interesting because the theory of such weak interactions is highly developed, and the interpretation of accurate experimental data is clear. Using the notation of Marshak, Riazzudin, and Ryan (1969), the current - current coupling of baryons to leptons is written $H = (G/\sqrt{2})(J_\mu^+ j_\mu + \text{h.c.})$. The phenomenological form of the baryon current for a decay like $\Sigma^- \rightarrow n e^- \bar{\nu}_e$ is

$$J_\mu = J_\mu^V + J_\mu^A, \tag{13}$$

$$J_\mu^V = \bar{\psi}_n (f_1 \gamma_\mu + (f_2/m_\Sigma)\sigma_{\mu\nu} q_\nu)\psi_\Sigma, \tag{14}$$

and

$$J_\mu^A = \bar{\psi}_n (g_1 \gamma_\mu \gamma_5 + (g_2/m_\Sigma)\sigma_{\mu\nu}\gamma_5 q_\nu)\psi_\Sigma \tag{15}$$

where J_μ^V and J_μ^A are the vector and axial vector parts, and $q_\lambda = (p_e + p_\nu)_\lambda = (p_\Sigma - p_n)_\lambda$ is the 4 - momentum of the

lepton pair. The terms f_1, f_2, g_1, g_2 are form factors, and can depend on q^2. The range is $m_e^2 \leq -q^2 \leq (m_\Sigma - m_n)^2$. The vector and axial vector form factors f_1 and g_1 are "large" compared to the weak magnetism and induced pseudo-tensor terms f_2 and g_2, which are multiplied by $\sim E_e/m_\Sigma$. In a $\Delta S = 0$ beta decay like $n \rightarrow pe^-\bar{\nu}_e$, the form factor $g_2 \neq 0$ would imply the existence of an axial vector current even under G parity, called "second" class" by Weinberg (1958). For $\Delta S = 1$ decays the I-spin rotation cannot be directly applied, and $g_2 \neq 0$ does not require second class currents, but g_2 should be no larger than $\sim (m_\Sigma - m_\Lambda)/m_\Sigma$.

3.4.2 Semileptonic Decay Experiments

The decay $\Sigma^- \rightarrow ne^-\bar{\nu}_e$ was studied in the Brookhaven negative hyperon beam by Tanenbaum et al (1975), and in the CERN negative hyperon beam by Decamp et al (1977). Both groups obtained $|g_1/f_1|$ by measuring the recoil neutron kinetic energy distribution. The Brookhaven group collected 3507 events, while the CERN group had 519 events. The Brookhaven group also collected 55 $\Sigma^- \rightarrow \Lambda e^-\bar{\nu}_e$ and 11 possible $\Sigma^- \rightarrow \Lambda e^-\bar{\nu}_e$. A second Brookhaven group running in the same hyperon beam obtained 127 $\Sigma^- \rightarrow \Lambda e^-\bar{\nu}_e$ and 15 $\Xi^- \rightarrow \Lambda e^-\bar{\nu}_e$ candidates (Herbert et al 1978). The results

of these experiments combined with previous world averages are shown in Table 3.

The experimental requirements for a high statistics study of $\Sigma^- \rightarrow ne^-\bar{\nu}_e$ are: (a) electron identification and momentum measurement; and (b) neutron detection. To select and reconstruct beta decay event candidates one must: (a) eliminate $\Sigma^- \rightarrow n\pi^-$ where a π^- is mistaken for an e^-; and (b) handle the neutron energy two-fold kinematic ambiguity.

The apparatus used by Tanenbaum et al is shown in Figure 2. Neutrons were detected by a downstream calorimeter composed of iron plates and multiwire proportional chambers. The neutron interaction point was determined to ±7 mm in this array. The neutron energy information was not sufficiently precise to provide a useful constraint. The proton counter was used to detect daughter $\Lambda \rightarrow p\pi^-$. Kink track events of the form $\Sigma^- \rightarrow$ negative particle in the fiducial region were reconstructed as two body decays $\Sigma^- \rightarrow n\pi^-$. The majority of such events were peaked at the Σ^- mass, and were caused by accidental fast muon counts in the Cerenkov counter in time with a beam $\Sigma^- \rightarrow n\pi^-$ decay. Time and space correlations between the scintillators that detected the negative and the signal from the appropriate Cerenkov counter segment were used to reduce the non-leptonic background. Further

reduction was achieved by requiring $m(n\pi^-) < 1165$ MeV/c^2. After final aperture cuts 3507 leptonic decay events remained.

The shape of the neutron energy spectrum is smeared by the kinematic ambiguity in neutron energy. Tanenbaum et al retained both solutions for the neutron energy, and used a maximum likelihood fit to a surface in $(E_n^{upper}, E_n^{lower})$ space. Their final result was $|g_1/f_1| = 0.435 \pm .035$.

The detection apparatus of Decamp et al at CERN used their DISC Cerenkov counter for Σ^- identification, a 2 m long threshold Cerenkov counter filled with a H_2-CH_4 mixture at atmospheric pressure for π^- rejection and e^- identification, a downstream neutron detector with optical spark chambers and iron plates, and two streamer chambers, one for the $\Sigma^- \rightarrow e^-$ kink, and one after an analyzing magnet for e^- momentum measurement. Event candidates reconstructed as $\Sigma^- \rightarrow n\pi^-$ showed a strong peak at the Σ^- mass, again due predominantly to accidentals in the H_2-CH_4 Cerenkov counter. A cut on low pulse height in the counter reduced the non-leptonic background substantially. The sample of beta decays was further purified by requiring $m(n\pi^-) < 1170$ MeV/c^2 and a low value of chi-squared for the hypothesis, $\Sigma^- \rightarrow ne^-\bar{\nu}_e$ calculated from the eight measured quantities

$\vec{p}_\Sigma$, $\vec{p}_e$, and $\vec{p}_n/|p_n|$. They estimated a residual background of 1.6% $\Sigma^- \to n\pi^-$ in the remaining 519 $\Sigma^- \to ne^-\bar{\nu}_e$ candidates. They weighted the two solutions for E_n equally in the analysis, and obtained $|g_1/f_1| = 0.17^{+.07}_{-.09}$ from a likelihood fit to the resulting neutron energy distribution. The CERN and Brookhaven results disagree by three standard deviations. This disagreement is reflected in the error assigned to this quantity in Table 3 by the Particle Data Group. The number $|g_1/f_1| = 0.385\pm.070$, is the world average of the two hyperon beam experiments plus several bubble chamber experiments each with less than 100 events.

Two groups at Brookhaven measured $\Sigma^- \to \Lambda e^-\bar{\nu}_e$. Herbert et al (1978) obtained a decay rate for this mode and for $\Xi^- \to \Lambda e^-\bar{\nu}_e$ as well. These rates, combined with previous work, are listed in Table 3. Tanenbaum et al (1975) measured f_1/g_1 for $\Sigma^- \to \Lambda e^-\bar{\nu}_e$ from the Λ energy distribution and angular correlation terms in the Σ^- rest frame for 55 events. The result is $f_1/g_1 = -0.25\pm0.35$ assuming $f_2 = 0$ and is quoted as the reciprocal of g_1/f_1 because it is expected that $f_1/g_1 \approx 0$ for this particular decay. This follows from the conserved vector current hypothesis, which predicts that $f_1/g_1 (\Sigma^- \to \Lambda e^-\bar{\nu}_e) \approx (m_\Sigma - m_\Lambda)/m_\Sigma$.

3.4.3 Search for the Rare Mode $\Xi^0 \to p\pi^-$

Geweniger et al (1975) have used the CERN neutral hyperon beam, where the Ξ^0 flux is about 1% of the Λ flux, to search for the $\Delta S = 2$ decay $\Xi^0 \to p\pi^-$. No decay which violates the selection rule $|\Delta S| \leq 1$ in first order weak interactions is known to exist, so a search for this process is of fundamental interest. A two body decay of this type is constrained, and the total momentum vector and mass of the parent particle can be determined from the vectors $\vec{p}_p$ and $\vec{p}_\pi$. The momentum of either particle in the Ξ^0 rest frame is 300 MeV/c, higher than that for any known decay mode of other particles in the neutral beam. It is an ideal candidate for a search for $\Delta S = 2$ decays, and a neutral hyperon beam is an ideal place to perform the search.

The group collected 10^9 events, corresponding to about 10^8 $\Lambda \to p\pi^-$, and roughly 10^6 beam Ξ^0's available to decay by the $\Delta S = 2$ mode. The major background at $m(p\pi) > 1250$ MeV/c^2 was found to be $K^0_S \to \pi^+\pi^-$ where the π^+ was assigned the proton mass. To eliminate these events the authors made a cut requiring $m(\pi\pi) > 550$ MeV/c^2. This cut also would have eliminated many $\Xi^0 \to p\pi^-$, and thus decreased their sensitivity to the decay mode. The limit they obtained, based on a signal of $\sim$ zero

events above a background of two events was $\Gamma(\Xi^0 \to p\pi^-)/\Gamma(\Xi^0 \to \Lambda\pi^0) < 3.6 \times 10^{-5}$ (90% confidence limit).

4 High Energy Hyperon Beams

4.1 Introduction

As mentioned in Section 2, it was anticipated that an order of magnitude increase in laboratory hyperon energy would substantially improve the signal to noise ratio in hyperon beams. The Fermilab program, reviewed by Sanford (1976), has included plans for neutral and charged hyperon beams since the first set of proposals was submitted to the laboratory. The neutral beam has been operating successfully for several years, and the charged beam is due to come on in 1979. In the meantime a similar accelerator has been built at CERN, the SPS, and a charged hyperon beam has been brought into operation there. The currently available results from these beams are reviewed below.

4.2 Fermilab Neutral Hyperon Beam

4.2.1 Experimental Apparatus

The layout of the Fermilab neutral hyperon beam is shown in Figure 8. Some of the characteristics of the beam are listed in Table 4. The hyperons were produced by a secondary proton beam, diffracted from the main beam

of the accelerator by the Meson Laboratory beryllium target, 450 m upstream of the apparatus. The proton energy equaled that of the accelerator - either 300 GeV or 400 GeV. The intensity could be varied from 10^6 - 10^{10} protons per pulse. The production angle could be varied between 0 and ±10 mrad by steering the proton beam in a vertical plane, keeping the axis of the collimator which defined the neutral beam fixed. The hyperons were produced in a 6 mm diameter metal target made of beryllium, copper, or lead. An ion chamber monitored proton intensity.

A brass collimator 5.3 m long in a vertical magnetic field defined the neutral beam and eliminated charged particles. The maximum $\int Bdl$ was 13.6 T m. The solid angle accepted by the collimator was 1.2 μ sr. All neutrals produced in this solid angle were transmitted to the downstream detectors. A typical beam Λ had momentum of 150 GeV/c and a decay length of 9.3 m, thus suffering small decay loss in the channel.

A veto counter defined the beginning of the decay volume, an 11 m vacuum pipe. Decays $\Lambda \to p\pi^-$, $K^o_S \to \pi^+\pi^-$, $\bar{\Lambda} \to \bar{p}\pi^+$ as well as $\gamma \to e^+e^-$ conversions and neutron interactions in the small amount of material in the beam were detected by a set of multiwire proportional chambers and an analyzing magnet. The device was designed to have high

acceptance for $\Lambda \rightarrow p\pi^-$. A threshold helium gas filled Cerenkov counter could distinguish protons and pions for those protons with momenta less than 170 GeV/c. No other mass measurements were made on secondary particles. A lead glass wall at the downstream end of the apparatus was used to detect γ rays from the decay sequence $\Xi^0 \rightarrow \Lambda\pi^0$, $\pi^0 \rightarrow \gamma\gamma$, $\Lambda \rightarrow p\pi^-$. From the momentum vectors $\vec{p}_+$ and $\vec{p}_-$ measured by the spectrometer the invariant mass of the parent $M_{+-} = [m_+^2 + m_-^2 + 2E_+E_- - 2\vec{p}_+ \cdot \vec{p}_-]^{1/2}$ was calculated using hypotheses $(m_+, m_-) = (m_p, m_\pi)$, (m_π, m_π), and (m_π, m_p) to search for Λ, K, and $\bar{\Lambda}$ respectively.

4.2.2 Inclusive Cross Sections

Extensive measurements were made of the spectra of neutral particles produced by 300 GeV protons at various laboratory angles on beryllium, copper and lead targets. The resulting invariant cross sections per nucleus for $p + Be \rightarrow \Lambda + X$ and $\bar{\Lambda} + X$ are shown in Figure 9 as a function of laboratory momentum for six angles between 0.25 mrad and 8.8 mrad. These figures are from Skubic et al (1978). The inclusive Λ spectra include daughter Λ's from Σ^0 decay, which could not be separated from "direct" Λ's. Note that at small angles the Λ spectra are rather flat as p_{lab} increases, indicating a leading particle effect, while the $\bar{\Lambda}$ spectra fall off very steeply with

increasing p_{lab}. At the lowest measured momentum, 60 GeV/c the ratio $\bar{\Lambda}/\Lambda = 0.1$. These data were fitted to smooth empirical functions of the scaling variables (x, $p_\perp$), and the lines shown on the figures were calculated from these fits. The fitted parameters are given in Table VI of Skubic et al (1978). Production data subsequently taken at 400 GeV show that $E\, d^3\sigma(x, p_\perp)/dp^3$ is independent of energy in this region. The $p_\perp$ dependences of the Λ and $\bar{\Lambda}$ spectra are similar - essentially $\exp(-2.3p_\perp^2)$, while the x dependences are very different. At $p_\perp = 0$, an expression of the form $Ed^3\sigma/dp^3 \sim (1-x)^n$ fits the data roughly, where $n_\Lambda = 0.6$, and $n_{\bar{\Lambda}} = 6.0$. These same data have been compared to the triple Regge model by Devlin et al (1977).

Inclusive cross sections for K_s, Λ, $\bar{\Lambda}$, and n produced by 200 GeV π^-, K^-, p^-, and p on beryllium have been measured by Edwards et al (1978) using the same beam line and detection apparatus. These results show remarkable similarities between the cross sections $\pi^- \to \Lambda$, $\pi^- \to \bar{\Lambda}$, and $p \to K_s$, between $\pi^- \to n$, and $K^- \to \Lambda$, and, to a lesser extent, between $\pi^- \to K_s$ and $p \to \Lambda$, and illustrate the insensitivity of the inclusive cross section to the particles involved.

4.2.3 A Dependence

Since invariant cross sections were measured for A production on copper and lead targets as well as beryllium, the dependence of the shape of the cross section on the atomic weight of the target nucleus (A dependence) could be studied. Interest in this subject has grown in recent years, because it may offer the possibility of studying the time development of a state of hadronic matter after a collision. A large number of particles are produced by a high energy interaction between two nucleons. Many of these particles are associated with the incident projectile, and are moving rapidly in the laboratory. In a heavy nucleus the time between collisions is so short that the definite number of particles observed in the asymptotic final state may not have time inside the nucleus to materialize. This picture has been discussed by Gottfried (1974), and was supported by the early work of Busza et al (1975), who showed that the forward angle multiplicity had very weak A dependence. Thus if a proton incident on a lead nucleus is excited by interaction with a target nucleon, this excited proton may travel through the rest of the nucleus and diffractively scatter, suffering a small loss in longitudinal momentum, and subsequently decay into the observed final state particles outside the nuclear volume.

The forward inclusive production of Λ's by protons was analyzed by Heller et al (1977) from this point of view. Following Busza et al (1975), these authors define the average number of absorption mean free paths encountered by an incident hadron h on a nucleus A as $\bar{\nu} = A\,\sigma_{hN}/\sigma_{hA}$, where σ_{hN} is the absorption cross section on a single nucleon target, and σ_{hA} is the corresponding cross section on nucleus A. Then taking experimental numbers $\sigma_{pN} = 33mb$, $\sigma_{pBe} = 216mb$, $\sigma_{pCu} = 812mb$, and $\sigma_{pPb} = 1930mb$ they calculate the values $\bar{\nu}_{Be} = 1.4$, $\bar{\nu}_{Cu} = 2.6$, and $\bar{\nu}_{Pb} = 3.6$. Thus copper is approximately one absorption length thicker than beryllium, and lead is one absorption length thicker than copper.

Figure 10 shows the differential multiplicity - the invariant cross section divided by σ_{hA} - for the three nuclear targets plotted as a function of rapidity y_c in the nucleon - nucleon center-of-mass. Note that as A increases the distribution at large y_c is depleted, as if the excited hadron lost energy by collision in leaving the nucleus. Although data were not taken between $y_c = 0$ and $y_c = 1.5$, the curves are suggestive of an enhancement at small y_c as A increases, thus leaving the multiplicities,

which are related to the areas under the curves, independent of A. A collision distribution function, quite similar to the inclusive proton distribution function in p + p → p + X, was found by Heller et al (1977) such that the copper shape was given by the distribution folded into beryllium, and the lead shape in turn was given by the same function folded into copper. The curves in Figure 10 thus support the definition of $\bar{\nu}$, and the view that an excited proton-like object scatters through the nucleus before materializing into the observed final state.

4.2.4 Polarization

Figure 8 shows that the Λ production angle could be varied in a vertical plane. A parity conserving strong interaction could produce a Λ polarization in the direction $\hat{n} = (\vec{p}_p \times \vec{p}_\Lambda)/|\vec{p}_p \times \vec{p}_\Lambda|$. A spin vector in this direction would be perpendicular to the magnetic field of the shield magnet M2 and would precess as the Λ moves through the collimator at a rate proportional to the magnetic moment.

The unexpected occurance of substantial Λ polarization was first reported by Bunce et al (1976). In this early work the precession was used to eliminate systematic errors in searching for a polarization effect. Since

parity is not conserved in the decay $\Lambda \to p\pi^-$, the proton distribution in the Λ rest frame is asymmetric if the parent Λ's are polarized, as discussed in Section 1. The relevant asymmetry parameter is given in Table 2. Reversing the direction of the magnetic field of M2 would reverse the longitudinal component of the polarization, without changing anything else, affording a technique to cancel out apparatus bias. The original 300 GeV measurements of the polarization have since been augmented by work at 400 GeV, reported by Heller et al (1978), and Figure 11 is taken from that reference. The Λ polarization is plotted as a function of Λ transverse momentum for Λ's produced by protons at the fixed laboratory angle of 7.2 mrad. The polarization increases monotonically with increasing $p_\perp$, and vanishes at $p_\perp = 0$. The direction of the polarization is along $-\hat{n}$, defined above. P_Λ reaches -0.25 at $p_\perp = 2$ GeV/c. It is not due to polarization of the incident proton beam, and is consistent with a parity conserving strong interaction in the reaction $p + Be \to \Lambda + X$. Preliminary data on $p + p \to \Lambda + X$ from hydrogen, reported by Grobel et al (1979) show that the polarization is not a complex nuclear effect. The fixed angle data of Figure 11 cannot be used to separate the kinematic dependence of P_Λ on x and $p_\perp$, since the two variables are uniquely related. Bunce et al

(1976) observed no noticeable x dependence in the 300 GeV data, which were taken at several angles between 0 and 9 mrad. Subsequent careful measurements at several production angles have shown that P_Λ does increase slightly with increasing x, as if it were associated in some way with the leading particle.

Figure 11 also shows the companion data on the polarization of $\bar{\Lambda}$'s. The maximum transverse momentum is smaller, but it is clear that $P_{\bar{\Lambda}} = 0$ for $p_\perp \leq 1$ GeV/c, and that $P_{\bar{\Lambda}}$ does not resemble P_Λ. This strengthens the notion that the polarization is a leading particle effect, since $\bar{\Lambda}$'s are not strongly associated with the incident proton. One more clue to the origin of this unexplained phenomenon has been supplied by Bunce et al (1979), who reported a polarization of Ξ° hyperons at 7.2 mrad production of $P_{\Xi^\circ} = -.086 \pm .019$, in agreement in sign and magnitude with the average P_Λ.

4.2.5 Magnetic Moments

The precession of the polarized Λ's in the magnetic field of M2 could obviously be exploited for a precise measurement of the Λ magnetic moment. This was done by Schachinger et al (1978). For hyperons with velocity $\approx$ c (a 75 GeV Λ has β = 0.99989) the precession angle is given in terms of the field integral by the formula ϕ (degrees) = (18.3) $\mu_\Lambda \int$Bdl (T m), where μ_Λ is measured in nuclear magnetons μ_N (units of e $\hbar$/2 m_pc). This angle was measured from the ratio of the transverse component to the longitudinal component of P_Λ after precession for various values of $\int$Bdl. Equal amounts of data were taken with the proton beam steered onto the beryllium target from above and from below the Λ line of flight, thus reversing P_Λ in space. Asymmetries for the two signs of production angle were then subtracted to eliminate instrumental bias. The resulting precession angles ϕ versus $\int$Bdl are plotted in Figure 12. The slope of the straight line gives the magnetic moment μ_Λ = -0.6138±0.0047 μ_N.

Λ hyperons which were daughters from the decay $\Xi^\circ \rightarrow \Lambda\pi^\circ$ were separated from Λ's produced by protons in the Be target by requiring the Λ momentum vector to intersect the plane of the target at a distance greater than 9 mm from the target center. The actual target radius was 3 mm, and no K_S° in the beam (which must be produced at the target) had a reconstructed distance greater than 6 mm. Λ's selected by this technique showed a growth curve in the decay vertex distribution characteristic of a parent - daughter decay. The 40,000 daughter Λ's selected in this manner were analyzed to measure spin direction in the same way as the beam Λ's. The daughter spin direction in turn gives the spin direction of the parent, and hence the precession angle of the Ξ°'s in the magnetic field. Analysis of ϕ versus $\int Bdl$ gave the result $\mu_\Xi = -1.20 \pm .06\ \mu_N$ (Bunce et al 1979).

The quark model discussed in Section 1 can be applied to the baryon magnetic moments. The baryons shown in Figure 1 are all composed of the three quarks (u, d, s). SU_6 gives a rule for combining the spins of the quarks to give the baryon spins: like quarks form spin 1. Thus the proton with spin up in this model would

have the structure $p\uparrow = \sqrt{2/3}\ (u\uparrow u\uparrow d\downarrow) - \sqrt{1/3}\ (d\uparrow(u\uparrow u\downarrow + u\downarrow u\uparrow)/\sqrt{2})$. The Σ^+, composed of (uus) has the same form. The Σ° (uds) is obtained by applying an I-spin lowering operator to Σ^+, which results in (ud) in a triplet state. The Λ is also (uds), but is orthogonal to Σ°, and hence has (ud) in a singlet state: $\Lambda\uparrow = s\uparrow(u\uparrow d\downarrow - u\downarrow d\uparrow)/\sqrt{2}$. In this model the spin and magnetic moment of the Λ are due entirely to the strange quark, and a measurement of μ_Λ is a measurement of μ_s. The magnetic moment of the u quark can be obtained from the proton moment by assuming that $\mu_u/\mu_d = -2$, the same as the charge ratio. This procedure gives a neutron moment about 3% smaller in magnitude than the experimental value. Taking $\mu_p = 2.7928$ and $\mu_\Lambda = -0.6138$ gives $\mu_u = 1.862$ and $\mu_s = -0.6138$ in nuclear magnetons. The masses of the constituent quarks can be calculated if $\mu_q = e_q \hbar/2m_q c$ is assumed, like Dirac "point" particles. The results $m_u = 336$ MeV/c^2 and $m_s = 510$ MeV/c^2 are in good agreement with quark mass differences and ratios calculated from observed splittings between particle masses in the various multiplets (see De Rujula, Georgi, and Glashow (1975) and Lipkin (1978)).

4.2.6 Elastic Scattering

A liquid hydrogen target 91 cm long was inserted in the neutral beam just upstream of the veto in Figure 8 to study Λp elastic scattering. The neutral beam flux was monitored by counting neutron conversions in a thin CH_2 slab placed upstream of the target. Unscattered beam Λ's and Λp scattering events were then detected for a fixed number of neutral beam counts to determine the cross section. Recoil protons emitted from the hydrogen target at large angles to the neutral beam were detected in two pairs of multiwire proportional chambers, one next to the target on the left side of the beam, and one on the right.

Given the scattered Λ momentum vector determined by $\Lambda \rightarrow p\pi^-$ and the recoil proton direction, the incident beam Λ momentum vector could be calculated, assuming the event to be elastic (a zero constraint fit). Inelastic background was eliminated by requiring the reconstructed beam Λ to point back to the beryllium production target in the same way as true beam Λ's. The details of the event selection, reconstruction, and normalization are discussed by Martin (1977). Proton - proton scattering was measured with the same apparatus by turning off M2 and bringing the proton beam through the neutral collimator to check the geometry and efficiency of the detector.

Figure 13 shows the elastic differential cross sections $d\sigma/dt$ for $\Lambda p \rightarrow \Lambda p$ (average energy 216 GeV) and $\bar{\Lambda} p \rightarrow \bar{\Lambda} p$ (average energy 120 GeV). The $\bar{\Lambda} p$ cross section has been divided by 10 to separate the points. The two cross sections are the same size, with essentially the same slope. The Λp cross section was fit by the expression $d\sigma/d|t| = Ae^{bt+ct^2}$, with $A = 50.2 \pm .75$ mb/(GeV/c)^2, $b = 10.06 \pm 0.11$ (GeV/c)$^{-2}$, and $c = 1.59 \pm 0.16$ (GeV/c)$^{-4}$. The $\bar{\Lambda} p$ cross section was fit by $A = 54.3 \pm 7.5$ mb/(GeV/c)^2, $b = 10.3 \pm 0.7$ (GeV/c)$^{-2}$, and $c = 0$. If the lower energy value of σ_T (Λp) = $34.6 \pm .4$ mb reported by Gjesdal et al (1972) is used as a guide, $A_{\Lambda p} = 61 \pm 0.7$ mb/(GeV/c)^2 is predicted by the optical theorem, 11 ± 1 mb above the measured result. As discussed in Section 3.3.3 an increase in the slope at small $|t|$ would decrease the discrepancy. The Λp cross section data were also divided into three separate momentum bins, centered at 134 GeV/c, 208 GeV/c, and 307 GeV/c, and the slopes were fit to each bin. These results for the effective slope at $|t| = 0.2$ GeV/c^2 are shown in Figure 14 together with the pp elastic cross section data and the lower energy $\Sigma^- p$ data from the charged hyperon beams.

4.3 CERN SPS Charged Hyperon Beam

4.3.1. Experimental Apparatus

The anticipated improvement in charged hyperon beam fluxes at higher energy was recently demonstrated by the CERN SPS charged hyperon beam (M. Bourquin et al submitted to Nuclear Physics B). At least three important new features were demonstrated by this beam. It is the first time that the feasibility of a positive hyperon beam has been demonstrated. Secondly, substantial fluxes of charged antihyperons were identified in the beam and thirdly, a flux of Ω^- sufficiently copious for detailed measurements of its properties was made available. Each of these features opens up a new experimental program.

This beam, which incorporated many design features of the earlier CERN beam, is shown in Figure 15a. Two superconducting quadrupole magnets and three bending magnets were used in the hyperon beam transport. Figure 15b shows the downstream detection apparatus, incorporating two DISC Cerenkov counters to count the hyperons directly and a magnetic spectrometer for the decay products. Under normal operating conditions only the SPS DISC counter was used for particle identification. At the downstream end of the

SPS DISC, a distance of 12.6m from the hyperon production target, the beam had a momentum bite $\Delta P/P = 10\%$, FWHM and a size of 1.5 x 2.0cm (h x v). A useful secondary beam intensity of about 10^6 particles could be achieved with 4×10^{10} protons incident on the hyperon production target. The background due to particles leaking through the shielding (mostly muons) was much less a problem than in the earlier charged hyperon beams; the secondary beam flux was limited only by the rate capabilities of the experimental apparatus.

The magnetic spectrometer played an essential role in identifying the rarer hyperons through their decays. It consisted of an analyzing magnet with a field integral of 2.2 T m with drift chambers on either side. The upstream chambers (DCI - DC4 of figure 15b) had a drift space of only 5mm to insure good resolution of close tracks as would occur from the decay $\Xi^- \rightarrow \pi^-\Lambda$ and the subsequent decay $\Lambda \rightarrow \pi^-p$. The chambers downstream of the magnet (DC5 - DC8) had a 1 cm drift distance since the tracks were now further apart.

Another very important feature of the spectrometer was its excellent photon and lepton detection capabilities. Wide angle photons were detected by the lead scintillator hodoscope before the magnet and more forward photons by lead glass and a lead and proportional chamber

array behind the magnet. This allowed the reconstruction of the decay $\bar{\Sigma}^+ \rightarrow \bar{p}\,\pi^\circ$ since both photons from the π° could be detected. The identification of $\bar{\Sigma}^+$ in a much larger sample of Σ^- was thus possible.

4.3.2 Hyperon Fluxes

Figure 16 is a DISC pressure curve taken at +100 Gev/c and shows a clean peak at the Σ^+ mass. The small Σ^+-$\bar{\Sigma}^-$ mass difference (8 Mev/c^2) is not resolved by the DISC. The flux of Σ^+ ($\bar{\Sigma}^-$) can be determined by reconstructing the decays $\Sigma^+(\bar{\Sigma}^-) \rightarrow n\ (\bar{n})\ \pi^+$. Since the Σ^+ and $\bar{\Sigma}^-$ lifetimes differ by a factor of two, (assuming $\tau_{\bar{\Sigma}} = \tau_{\Sigma}$) they will have different distributions of their decay vertices. Fitting to this vertex distribution and making cuts involving the Σ^+ - $\bar{\Sigma}^-$ mass difference allows a determination of the $\bar{\Sigma}^-/\Sigma^+$ production ratio. The flux of $\bar{\Xi}^-$ was too small to be seen as a peak in the DISC curve since the DISC background levels were 10^{-7} to 10^{-6} of the total beam flux through it. However, by triggering with the DISC set to the Ξ mass and then fitting to the decay $\bar{\Xi}^- \rightarrow \bar{\Lambda}\,\pi^+$ and $\bar{\Lambda} \rightarrow \bar{p}\,\pi^+$, a clean identification could be made. The corresponding reconstructed Ξ^- and Λ masses have widths of 6 and 4 MeV/c^2 (FWHM) respectively. The dashed curve of Figure 16 shows the expected Ξ^- signal based on events reconstructed in this way.

The Ω^- flux, although also too small to be seen as a peak in the DISC pressure curve could be readily measured by reconstructing the decay $\Omega \rightarrow K^- \Lambda$, $\Lambda \rightarrow \pi^- p$. The major background was due to the topologically similar Ξ^- decay but simple mass cuts allowed good separation. For 10^6 beam particles identified by the DISC, typical running conditions at -100 GeV/c provided 4000 Σ^-, 2 $\bar{\Sigma}^+$, 400 Ξ^-, and 0.1 Ω^-. For +100 GeV/c 46 Σ^+, 4 $\bar{\Sigma}^-$, and 2 $\bar{\Xi}^-$ were typical fluxes.

Bourquin et al compared particle production ratios as a function of strangeness at $x_\pi = 0.48$. The variable x_π is the Feynman x of the beam pions. The ratios are plotted in Figure 17 and display a number of interesting patterns. The decreasing strange baryon production cross section as compared to pions is demonstrated by the decrease by a factor of 50 - 100 of this ratio for each unit change of baryon strangeness. As has been noted for Λ and $\bar{\Lambda}$ yields, two production mechanisms are probably at work. At large values of x the baryons are produced diffractively giving rise to the leading particle effect, while at smaller x values the production of baryon - anti-baryon pairs is significant. The figure shows that the diffractive production of strange baryons becomes progressively less dominant as the strangeness of the baryon increases.

4.3.3 Ω^- Properties

Measurements of the Ω^- lifetime by the early bubble chamber experiments were severely limited by statistics, but clustered about a value of 1.3×10^{-10} seconds. Three bubble chamber experiments with larger event samples have recently been reported. A measurement of Deutschmann et al (1978) using 101 events produced by 10 and 16 GeV/c K^- yielded a lifetime of $\tau = 1.41^{+.15}_{-.24}.10^{-10}$ sec in agreement with the earlier bubble chamber results. The measurement of Hemingway et al (1978) with 40 Ω^- produced by 4.2 GeV/c K^- gives $\tau = 0.75^{+.14}_{-.11}.10^{-10}$ sec and that of Baubillier et al (1978) using 41 events produced by 8.25 GeV/c K^- yields $\tau = 0.80^{+.16}_{-.12}.10^{-10}$ sec. The measurement of Hemingway et al is claimed to be particularly free of biases since their data is just above the Ω^- production threshold and used only events where the production kinematics were over constrained (no missing neutral particles) to help separate the Ω^- from the much more copious, and topologically similar, Ξ^- decays. This was not possible for the other measurements because of their higher energy.

The hyperon beam measurement of Bourquin et al, (1978) used a sample of 1410 Ω^- which decayed by the mode $\Omega^- \rightarrow \Lambda K^-$ and $\Lambda \rightarrow \pi^- p$. They estimate their background as 23 events, about half of which are due to another Ω^- decay mode and the rest due to misidentified Ξ^- decays. The best fit to

the data yields a preliminary lifetime of $0.82 \pm 0.06.10^{-10}$ sec in good agreement with Hemingway et al (1978) and Baubillier et al (1978).

Bourquin et al (1978) measured the Ω^- decay branching ratios and the α parameter for the decay $\Omega^- \rightarrow \Lambda K^-$. These are given in Table 2. The ratio of the decay $\Omega \rightarrow \Xi^0\pi^-$ to $\Omega^- \rightarrow \Xi^-\pi^0$ is predicted to be equal to 2 for a pure $\Delta I = 1/2$ amplitude. This same group also find three possible candidates for the leptonic decay of the Ω^-. The analysis is still preliminary but these events would correspond to a $\sim$1% leptonic branching ratio.

4.4 The Fermilab Charged Hyperon Beam

The charged hyperon beam under construction at Fermilab is designed to target the primary 400 GeV proton beam at fluxes of up to 10^{12} protons per pulse. The main component of the hyperon channel is a large dipole magnet, 7m in length, and capable of 3.5T. The channel itself is designed to operate over a momentum range of 100 - 350 GeV/c. Figure 18 a and b show the expected positive and negative particle fluxes at a distance of 10m from the production target. Flux estimates for this beam have been made by Doroba (1978); the above figure incorporate the recent flux measurements of Bourquin et al (submitted to Nuclear Physics 1978). The figures assume that the

incident proton beam is adjusted to give 10^6 secondary particles emerging from the channel. These hyperon fluxes are very substantial and in the high momentum range of the negative beam, hyperons become the dominant particles. The approved program for this beam will include a new particle search, a hyperon flux and polarization measurement, and a measurement of hyperon elastic scattering.

5. Future Prospects

At this time two hyperon beams are operational, a neutral beam at Fermilab and a charged beam at CERN. Within a year a new charged hyperon beam will be completed at Fermilab capable of exploiting a considerably higher energy and intensity range than the existing beams. The utilization of these beams in the next few years should provide significant advances in a number of areas.

Systematic measurements of Λ and $\bar{\Lambda}$ production cross sections over a wide range of kinematic variables have been published, and a high statistics study of Ξ^0 production, including A dependence and polarization, has been completed. Similar measurements for the charged hyperons are either planned or already in progress. The behavior of the Λ polarization as a function of $p_\perp$ out to 6 GeV/c is planned for the Fermilab neutral beam.

Precision measurements of the static properties of the hyperons have been demonstrated by the recent hyperon beam measurements of the Ω^- lifetime and the Λ and Ξ^0 magnetic moments and have obvious extensions to the other hyperons. Only the high energy charged beams have sufficient fluxes of Ω^- to make significant advances in the study of its branching ratios and other static properties. Almost all previous knowledge of antihyperon properties has come from bubble chamber measurements and had limited statistical impact. The significant fluxes of antihyperons in the SPS and Fermilab high energy hyperon beams should allow measurements of their static properties and tests of CP and CPT with much greater precision.

The semileptonic decays of hyperons present a unique handle on the fundamental parameters of weak interaction theory. These decays are experimentally very challenging but measurements made with the early CERN and BNL demonstrate that they can be done. The much higher fluxes available with the higher energy beams coupled with modern detector technology should provide for better control of systematic errors and allow the extension of these measurements to a wider group of decays. A high statistics study of polarized $\Lambda^0 \rightarrow pe^-\bar{\nu}_e$ will be done in the FNAL neutral beam. The existing discrepancy in the decay

$\Sigma^- \rightarrow n\, e^- \bar{\nu}$ noted in section 3.4.2 should be resolved and a much more accurate (and hopefully consistent) set of decay parameters will be attainable. The possiblity of making measurements of the Ω^- leptonic decays is a particularly intriguing since no measurements of the weak decays of any member of the baryon decouplet now exist.

Hyperon beams provide the only means for measuring the strong interaction properties of the hyperons. Again the early hyperon beams showed the feasibility of measuring total and differential cross sections, and the diffractive excitation of hyperons. Because hyperons are convenient analysers of the spin configuration of their final state, they have unique advantages in helping to understand hadronic excited states. This field is totally unexplored at high energies.

We are pleased to acknowledge helpful and frank discussions with many of our colleagues engaged in hyperon research.

REFERENCES

Akerlof, C. W. et al, 1976. Phys. Rev. D14:2864

Allaby, J. V. et al, 1970. CERN Report No. 70-12

Anderson, K. J. et al, 1975. Phys. Rev. 11D:473

Arik, Engin 1976, Inclusive Lambda Production in Sigma-Proton Collisions at 23 GeV/c, PhD Thesis, University of Pittsburgh, Pittsburgh, PA 58pp

Armenteros, R. Barker, K. H., Butler, C. C. Cachor, A., 1951. Phil. Mag. 42:1113

Ayres, D. S. et al, 1977. Phys. Rev. 15D:3105

Badier, J. et al, 1972a. Phys. Lett. 39B:414

Badier, J. et al, 1972b. Phys. Lett. 41B:387

Barbiellini, G. et al, 1972. Phys. Lett. 39B:663

Baubillier, M. et al, 1978. Phys. Lett. 78B:342

Blaising, Jean-Jacques, 1977. Interactions Hadroniques Des Hyperons Sigma Minus A 17 GeV. PhD Thesis. Universite Louis Pasteur. Strasbourg, France. (In French.)

Blaising, J. J. et al, 1975. Phys. Lett., 58B:121

Boggild, H. Ferbel, T., 1974. Ann. Rev. Nucl. Sci. 24:451

Bourquin, M. et al, 1978. Contributed Paper to the 19th International Conference on High Energy Physics (Session B7E), Tokyo

Bruneton, C. et al, 1977. Nucl. Phys. B124:391

Bunce, G. et al, 1976. Phys. Rev. Lett. 36:1113

Bunce, G. et al, 1978. Phys. Rev. D18:633

Bunce, G. et al, 1979. Bull. Am. Phys. Soc. 24:46

Burq, J. P. et al, 1978. CERN EP Internal Report 78-7

Busza, W. et al, 1975. Phys. Rev. Lett. 34:836

Cabibbo, N. 1963. Phys. Rev. Lett. 10:531

Chinowsky, W. 1977. Ann. Rev. Nucl. Sci. 27:393

Coleman, S., Glashow, S. L. 1961. Phys. Rev. Lett. 6:423

Dalitz, R. H. 1957. Rep. Prog. Phys. 20:163

Decamp, D. et al, 1977. Phys. Lett. 66B:295

De Rujula, A., Georgi, H., and Glashow, S. 1975. Phys. Rev. D12:147

Deutschmann, M. et al, 1978. Phys. Lett. 73B:96

Devlin, T. et al, 1977. Nucl. Phys. B123:1

Doroba, K. 1978. Fermilab TM-818

Dreitlein, J., Primakoff, H. 1962. Phys. Rev. 125:1671

Dydak, F. et al, 1977. Nucl. Phys. B118:1

Edwards, R. T. et al, 1978. Phys. Rev. D18:76

Eichten, T. et al, 1972. Nucl. Phys. B44:333

Gell-Mann, M. 1953. Phys. Rev. 92:833

Gell-Mann, M. 1961. Cal. Tech. Report CTSL-20

Gell-Mann, M. 1964. Phys. Lett. 8:21

Gell-Mann, M., Rosenfeld, A. H. 1957. Ann. Rev. Nucl. Sci. 7:407

Geweniger, C. et al, 1974. Phys. Lett. 48B:483

Giacomelli, G. 1976. Phys. Reports 23C:123

Gjesdal, S. et al, 1972. Phys. Lett. 40B:152

Glauber, R. J. 1960. International Conference on Nuclear Forces and the Few Nucleon Problem, Ed. Griffith, T. C., Power, E. A., Vol. 2. New York: Pergamon.

Gotteried, K. 1974. Phys. Rev. Lett. 32:957

Grobel, R. 1979. Bull. Am. Phys. Soc. 24:46

Harrington, D. R. 1964. Phys. Rev. 135:B358

Heller, K. et al, 1977. Phys. Rev. D16:2737

Heller, K. et al, 1978. Phys. Rev. Lett. 41:607

Hemingway, R. et al, 1978. Nucl. Phys. B142:205

Herbert, Marc Louis, 1978. Measurement of Sigma-Minus Decay to Lambda, Electron, and Neutrino and SI-Minus Decay to Lambda, Electron, Neutrino Branching Ratios, PhD Thesis, University of Pittsburgh, Pittsburgh, PA 194pp

Herbert, M. L. et al, 1978. Phys. Rev. Lett. 40:1230

Holder, M. et al, 1971. Phys. Lett. 36B:400

Hungerbuhler, Viktor M. 1973. Production of Negative Hyperon Resonances and Omega Minus By Sigma Minus and XI Minus at 24.6 GeV/c. PhD Thesis. Yale University, New Haven, CT 106pp

Hungerbuhler, V. et al, 1974a. Nucl. Instr. Meth. 115:221

Hungerbuhler, V. et al, 1974b. Phys. Rev. D10:2051

Hungerbuhler, V. et al, 1975. Phys. Rev. D12:1203

Jensen, D. A. et al, 1969. Phys. Rev. Lett. 23:615

Lach, J. 1977. Proceedings of the Twelfth Recontre De Moriond, Flaine, Vol. 2. pp 13-36

Lipkin, H. 1975. Particles and Fields, 1975. APS/DPF Seattle, pp 352

Lipkin, H. 1976. Proceedings of the Eleventh Roncontre De Moriand, Flaine, Vol. 1, pp 169-185

Lipkin, H. 1978. Phys. Rev. Lett. 41:1629

Lipkin, H. J., Scheck, F. 1966. Phys. Rev. Lett. 16:71

Litt, J., Meunier, R. 1973. Ann. Rev. Nucl. Sci. 23:1

Majka, Richard Daniel 1974. Sigma Minus-Proton Elastic Scattering at 23 GeV/c. PhD Thesis. Yale University, New Haven, CT. 125pp

Majka, R. et al, 1976. Phys. Rev. Lett. 37:413

Marshak, R. E., Riazuddin, Ryan, C. P. 1969. Theory of Weak Interactions in Particle Physics. New York: Wiley-Interscience

Martin, Philip Scott, 1977. Lambda-Proton Elastic Scattering at 23 GeV/c. PhD Thesis. University of Wisconsin-Madison. Madison, WI 113pp

Neeman, Y. 1961. Nucl. Phys. 26:222

Overseth, O. E. 1976. Rev. Mod. Phys. 48:5242

Overseth, O. E., Pakvasa, S. 1969. Phys. Rev. 184:1663

Paticle Data Group, 1978. Phys. Lett. 75B:1

Quigg, C., Rosner, J. L. 1976. Phys. Rev. 14D:160

Rochester, G. D., Butler, C. C. 1947. Nature 160:855

Samios, N. P., Goldberg, M., Meadows, B. T. 1974. Rev. Mod. Phys. 46:49

Sandweiss, J. 1971. Proceedings of the International Conference on Instrumentation for High Energy Physics, Dubna:717

Sanford, J. 1976. Ann. Rev. Nucl. Sci. 26:151

Schachinger, L. et al, 1978. Phys. Rev. Lett. 41:1348

Skubic, R. et al, 1978. Phys. Rev. D18:3115

Tanenbaum, W. et al, 1974. Phys. Rev. Lett. 33:175

Tanenbaum, W. et al, 1975. Phys. Rev. D12:1871

Wang, C. L. 1970. Phys. Rev. Lett. 25:1068

Weinberg, S. 1958. Phys. Rev. 112:1375

Willis, W. J. et al, 1971. Nucl. Instr. And Meth. 91:33

Zweig, G. 1964. CERN Report 8409/TH412

Figure Captions

1. The lowest mass $1/2^+$ octet representation and $3/2^+$ decuplet representation of the baryons.
2. The configuration of the BNL charged hyperon beam showing in detail the beam dump region and the beam channel Cerenkov counter with high resolution spark chamber.
3. The CERN charged hyperon beam. Note that the two superconducting quadrupoles fit snugly between the coil of the dipoles and take little extra space.
4. Invariant cross sections for Σ^- and Ξ^- production by protons on beryllium as a function of x. These data are from Hungerbuhler et al (1975) and Badier et al (1972a). Production cross sections of other particles taken from Allaby et al (1970) are shown for comparison. Note the differences in incident momentum and production angle.
5. The apparatus of Dydak et al (1977) used to measure the Σ^0 lifetime.
6. A comparison of the Σ^-p elastic scattering cross sections from the CERN and BNL charged hyperon beams.
7. The data of Dydak et al (1977) used to extract the Σ^0 lifetime. The Primakoff effect peak is clearly visible at small q^2.

8. Layout of the Fermilab neutral hyperon beam. The magnet M1 restored the proton beam to the production target T. M2 was the neutral beam collimator and charged particle sweeping magnet. Decays were observed after the veto by MWPC's C1 - C6 and the analyzing magnet M3.
9. Invariant Cross Sections at 300 GeV taken from Skubic et al (1978).
   a) $p + Be \rightarrow \Lambda/\Sigma^{\circ} + X$
   b) $p + Be \rightarrow \bar{\Lambda} + X$
10. Differential multiplicities for Λ production at 0 mrad from Be, Cu, and Pb taken from the paper by Heller et al (1977).
11. Polarization of Λ and $\bar{\Lambda}$ produced by 400 GeV protons on beryllium taken from the work of Heller et al (1978).
12. The Λ precession angle as a function of the magnetic field integral from Schachinger et al (1978).
13. Λp and $\bar{\Lambda} p$ elastic scattering cross sections from the Fermilab neutral hyperon beam. The $\bar{\Lambda} p$ cross section have been multiplied by 1/10 to facilitate plotting.

14. A compilation of elastic scattering b parameters evaluated at $t = 0.2$ $(GeV/c)^{-2}$ for hyperon proton scattering. Selected pp data is shown for comparison (Giacomelli 1976).
15. The CERN SPS charged hyperon beam. The magnetic beam transport elements are shown in (a) and the layout of the magnetic spectrometer is shown in (b).
16. A DISC pressure curve taken for positive particles with the SPS hyperon beam.
17. Particle production ratios as a function of strangeness from Bourquin et al submitted to Nuclear Physics B.
18. Flux estimates for the Fermilab charged hyperon beam. The data points represent the range in x of measurements made with other charged hyperon beams. See Doroba (1978) for details.

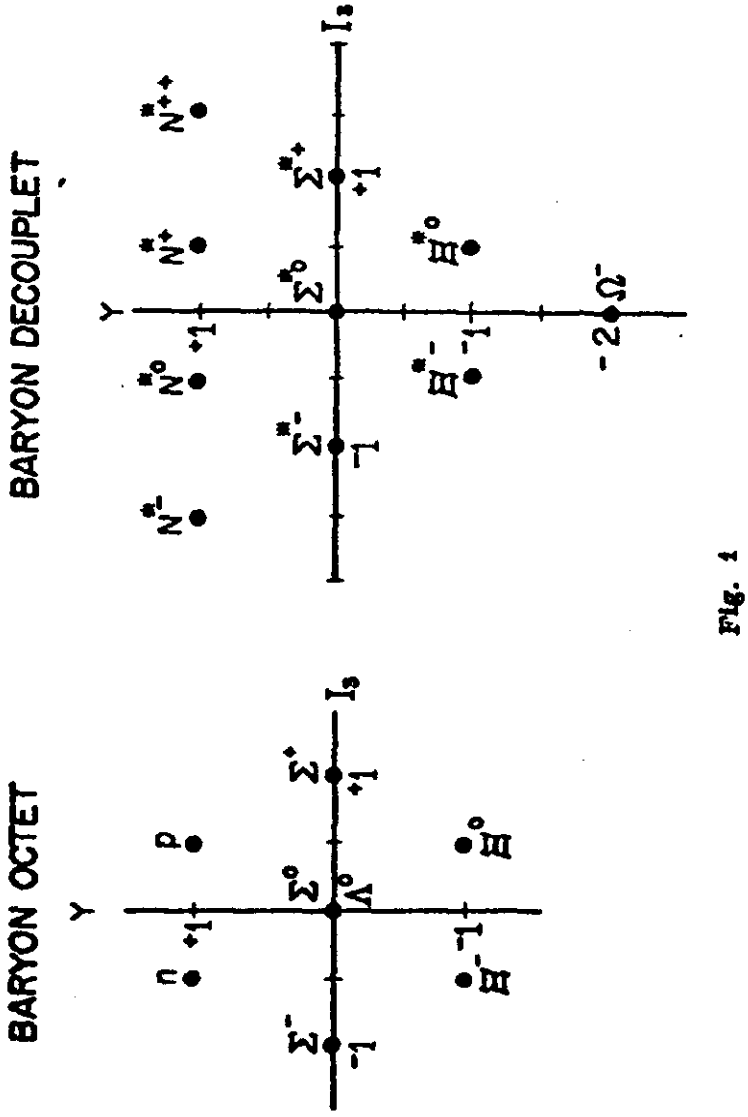
BARYON DECOUPLET
BARYON OCTET
Y
I_3
+1
-1
-2
N^{*++}
N^{*+}
N^{*0}
N^{*-}
Σ^{*+}
Σ^{*0}
Σ^{*-}
Ξ^{*0}
Ξ^{*-}
Ω^-
p
n
Σ^+
Σ^0
Σ^-
Λ^0
Ξ^0
Ξ^-

Fig. 1

HIGH ENERGY NEGATIVE HYPERON BEAM

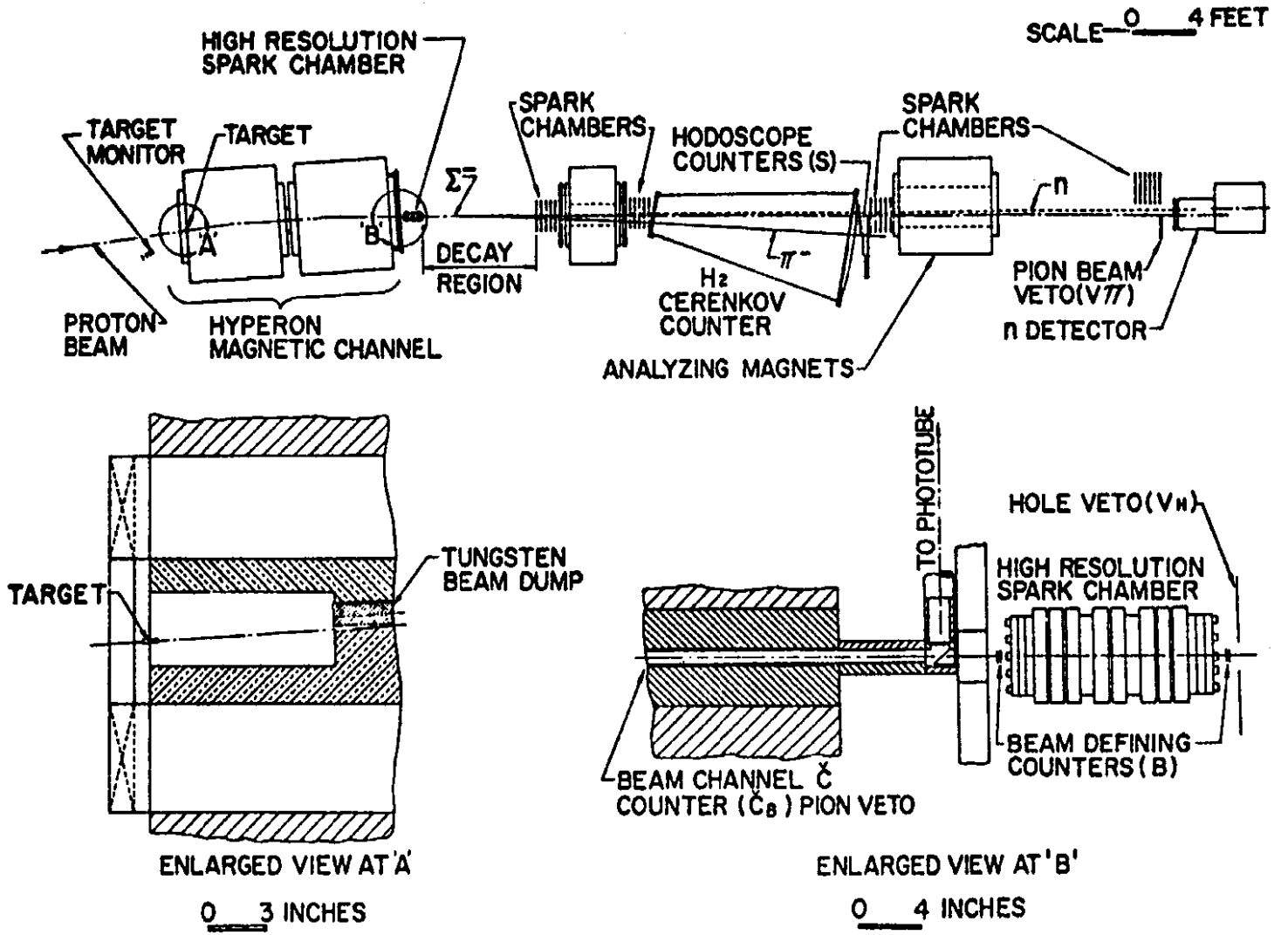

Fig. 2

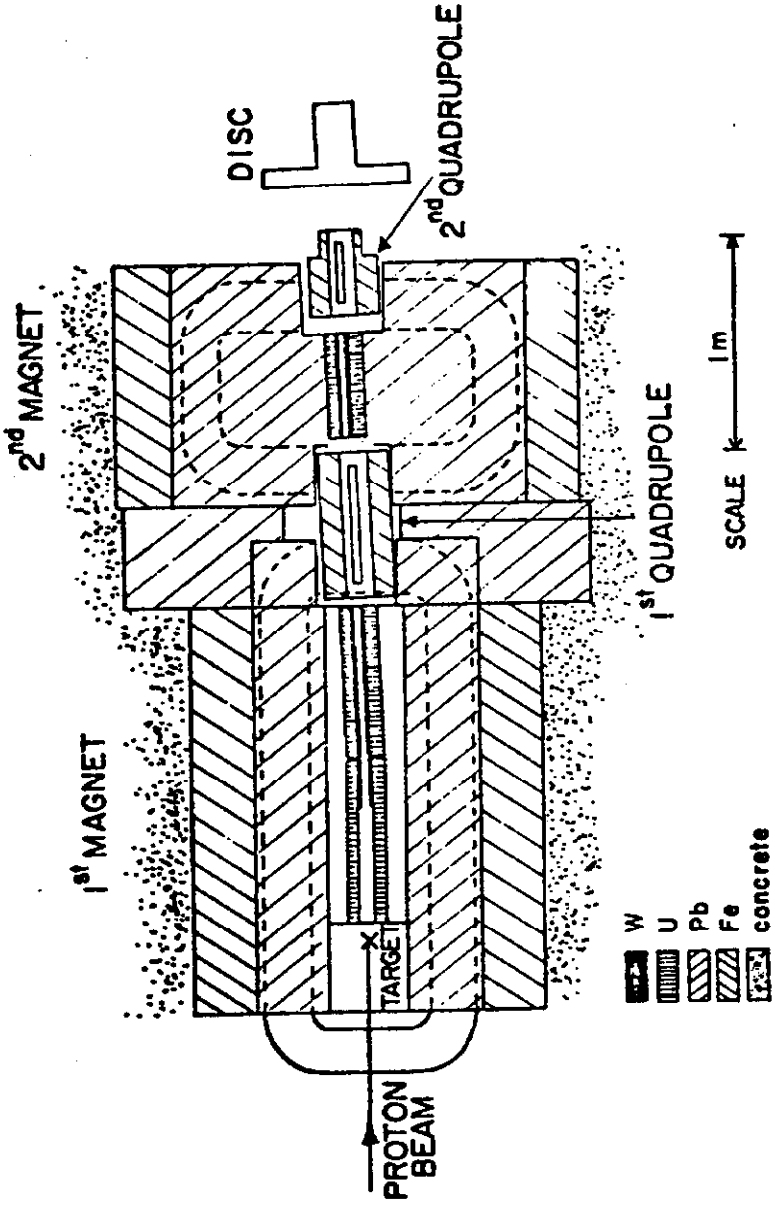
DISC
2nd QUADRUPOLE
2nd MAGNET
1st QUADRUPOLE
1st MAGNET
SCALE
1m
W
U
Pb
Fe
concrete
TARGET
PROTON BEAM

Fig. 3

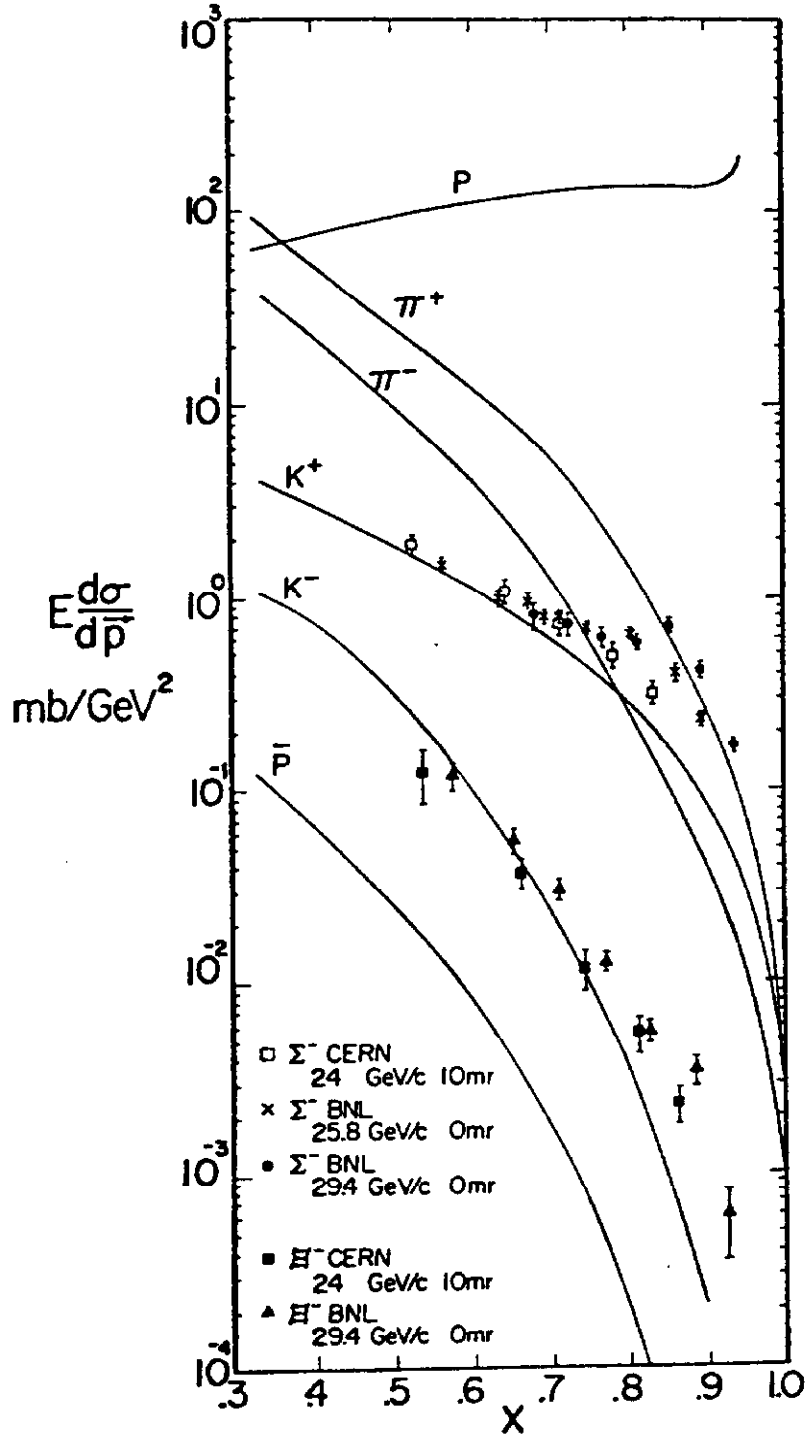
$E\frac{d\sigma}{d\vec{p}}$
mb/GeV^2
10^3
10^2
10^1
10^0
10^{-1}
10^{-2}
10^{-3}
10^{-4}
P
π^+
π^-
K^+
K^-
$\bar{P}$
□ Σ^- CERN 24 GeV/c 10mr
× Σ^- BNL 25.8 GeV/c 0mr
• Σ^- BNL 29.4 GeV/c 0mr
■ Ξ^- CERN 24 GeV/c 10mr
▲ Ξ^- BNL 29.4 GeV/c 0mr
.3
.4
.5
.6
.7
.8
.9
1.0
X

Fig. 4

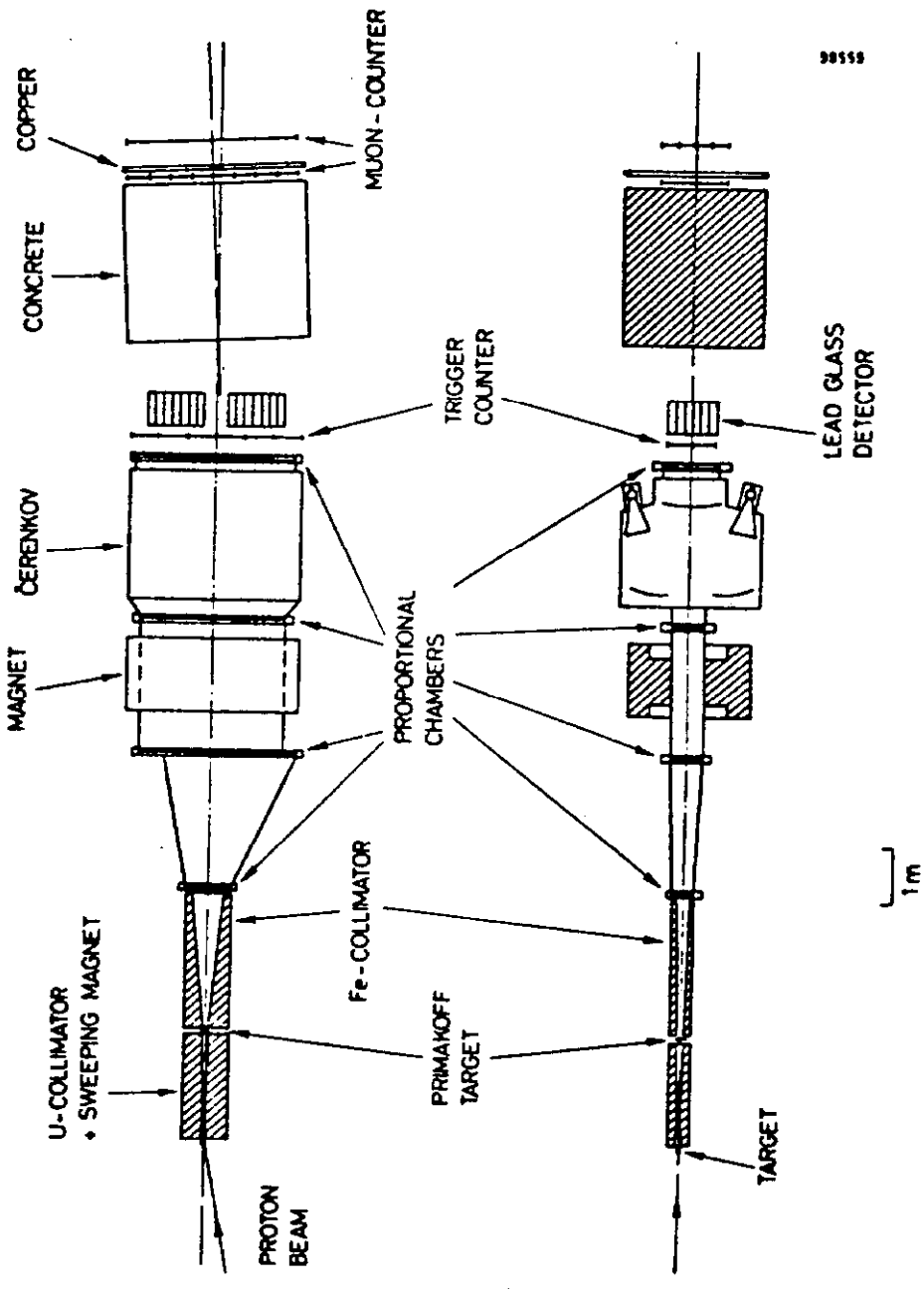
COPPER
MUON - COUNTER
CONCRETE
TRIGGER COUNTER
LEAD GLASS DETECTOR
ČERENKOV
MAGNET
PROPORTIONAL CHAMBERS
Fe - COLLIMATOR
U-COLLIMATOR + SWEEPING MAGNET
PRIMAKOFF TARGET
PROTON BEAM
TARGET
1m

Fig. 5

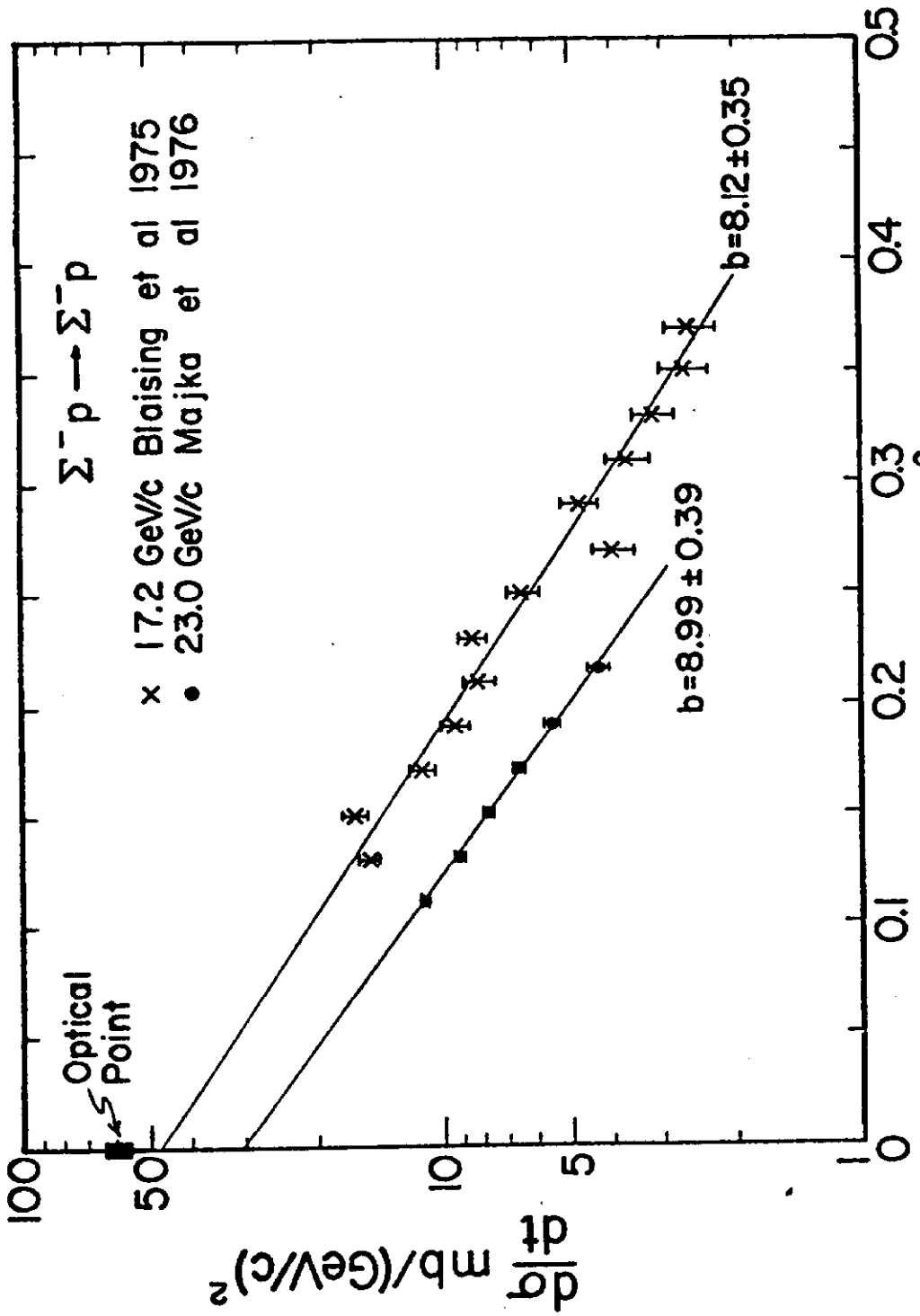
$\Sigma^- p \rightarrow \Sigma^- p$
× 17.2 GeV/c Blaising et al 1975
• 23.0 GeV/c Majka et al 1976
b=8.12±0.35
b=8.99±0.39
Optical Point
$\frac{d\sigma}{dt}$ mb/(GeV/c)^2
$-t$ (GeV/c)^2
100
50
10
5
1
0
0.1
0.2
0.3
0.4
0.5

Fig. 6

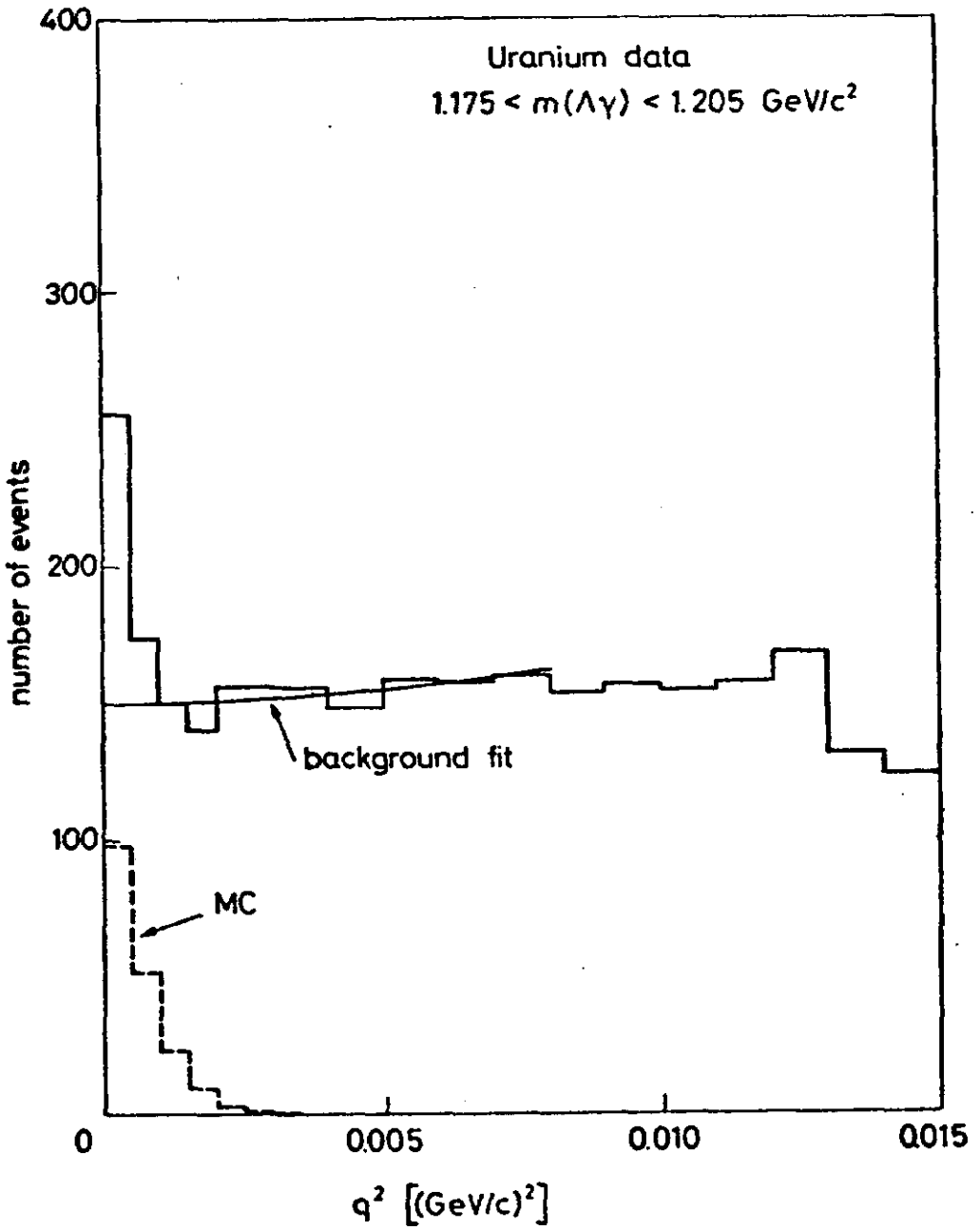
Uranium data
1.175 < m(Λγ) < 1.205 GeV/c²
number of events
400
300
200
100
0
0.005
0.010
0.015
background fit
MC
q² [(GeV/c)²]

Fig. 7

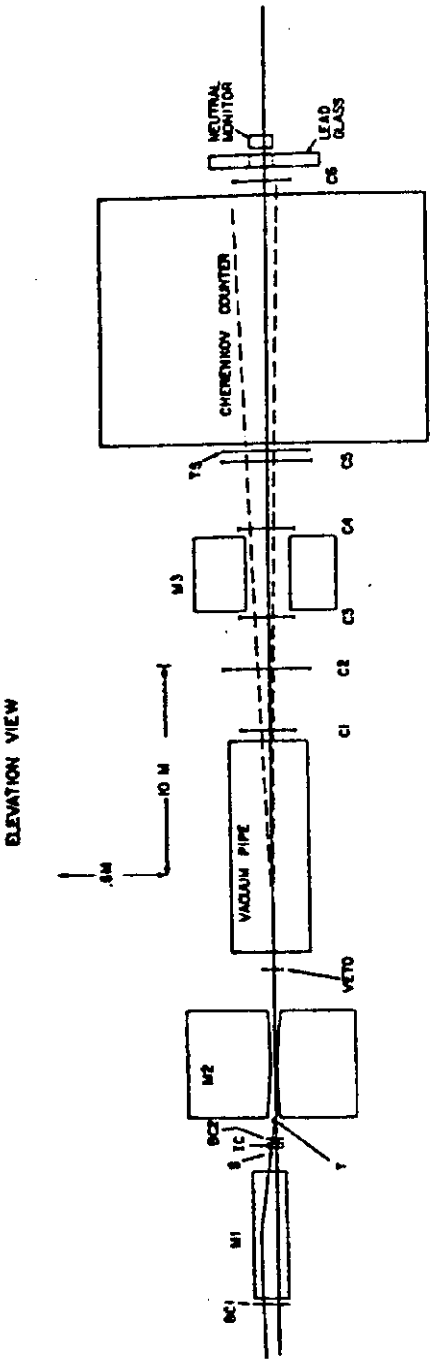
ELEVATION VIEW
10 M
NEUTRAL MONITOR
LEAD GLASS
C6
CHERENKOV COUNTER
T6
C5
C4
M3
C3
C2
C1
VACUUM PIPE
VETO
M2
SC2
T2
T1
M1
SC1

Fig. 8

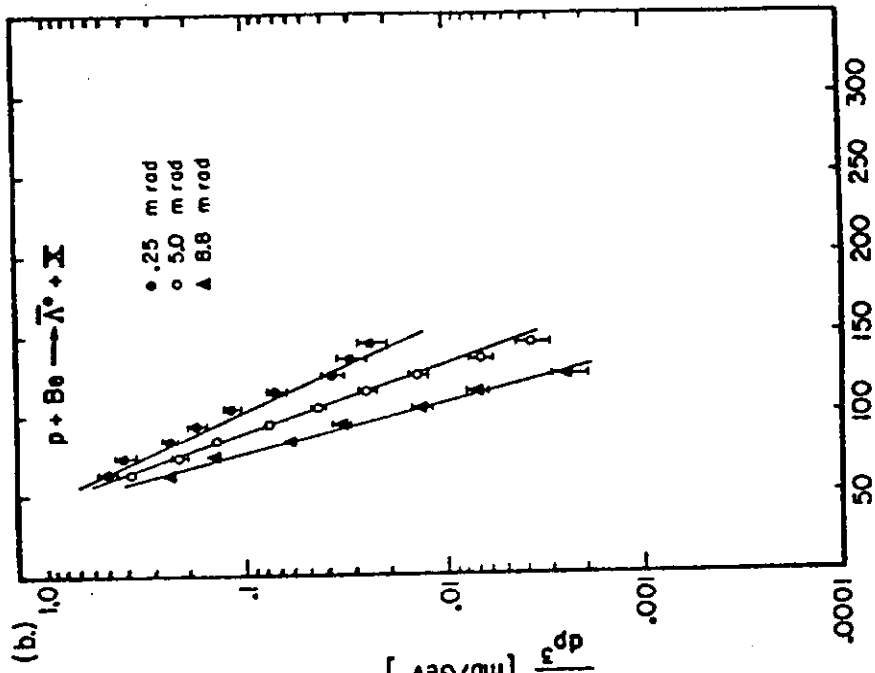
(b.)
p + Be → $\bar{\Lambda}^0$ + X
• .25 m rad
○ 5.0 m rad
▲ 8.8 m rad
$\frac{Ed^3\sigma}{dp^3}$ [mb/GeV^2]
P_{lab} [GeV/c]

Fig. 9(b)

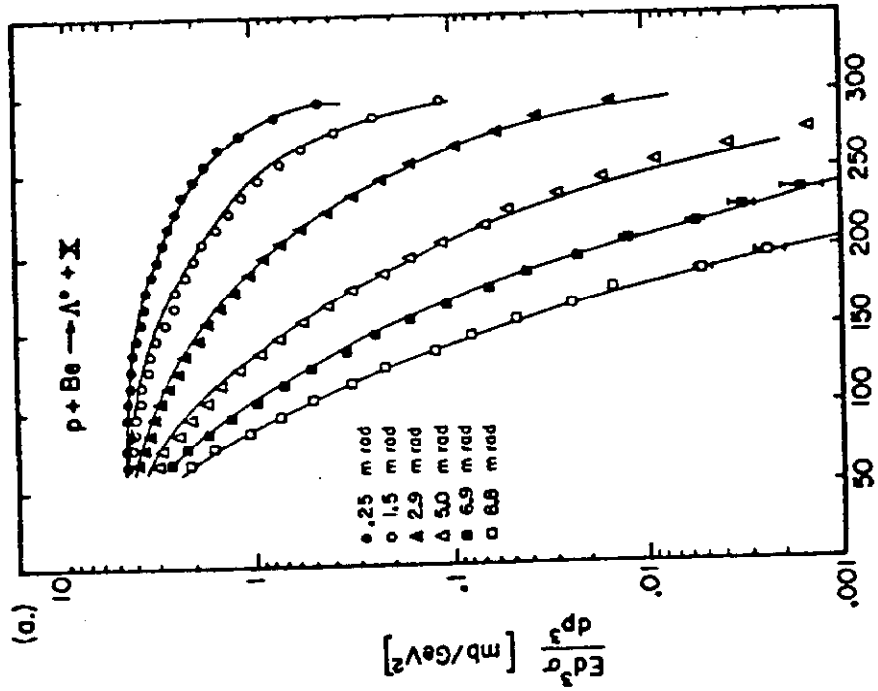
(a.)
p + Be → Λ^0 + X
• .25 m rad
○ 1.5 m rad
▲ 2.9 m rad
△ 5.0 m rad
■ 6.9 m rad
□ 8.8 m rad
$\frac{Ed^3\sigma}{dp^3}$ [mb/GeV^2]
P_{lab} [GeV/c]

Fig. 9(a)

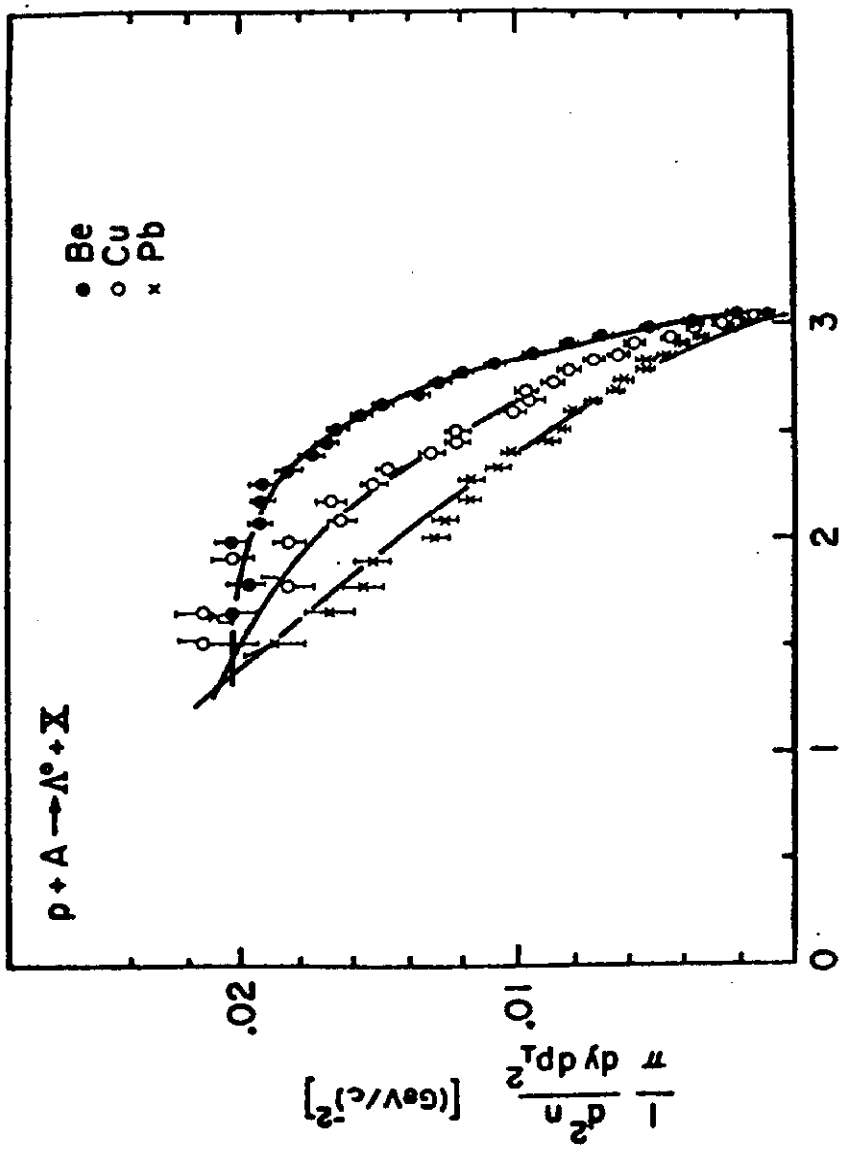

Fig. 10

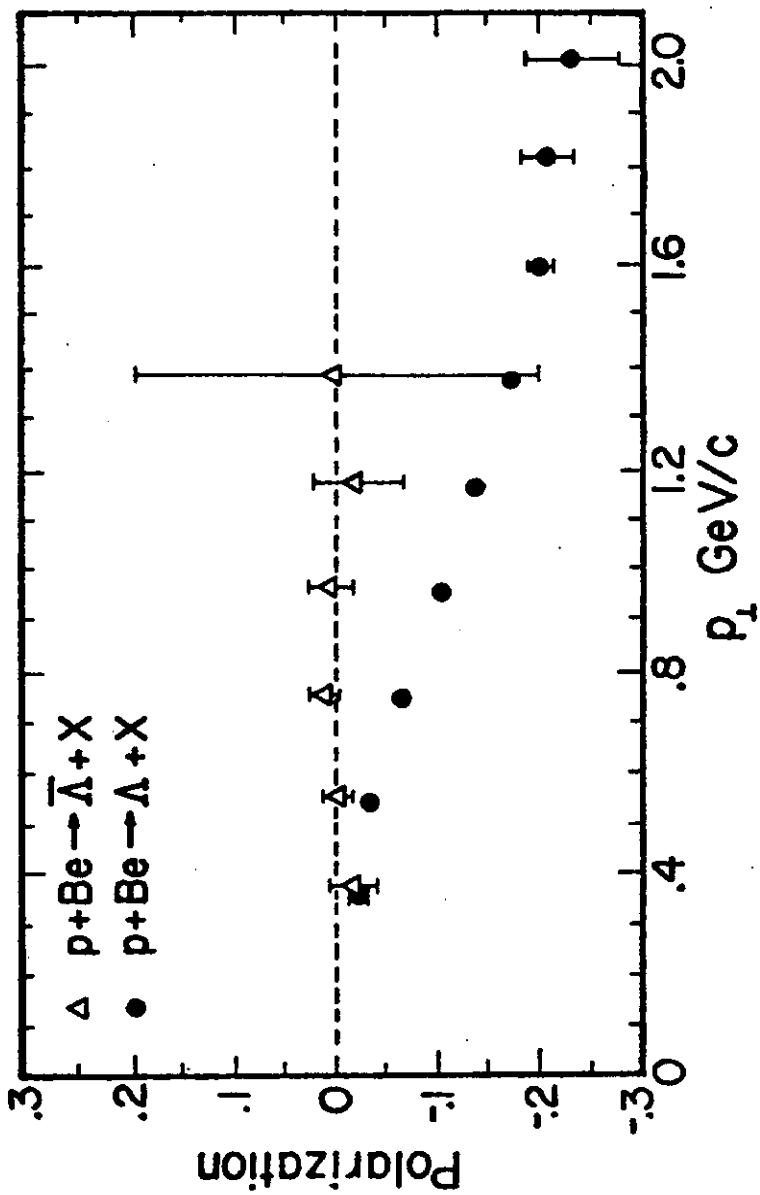
Polarization
.3
.2
.1
0
-.1
-.2
-.3
0
.4
.8
1.2
1.6
2.0
$p_\perp$ GeV/c
p+Be→$\bar{\Lambda}$+X
p+Be→Λ+X

Fig. 11

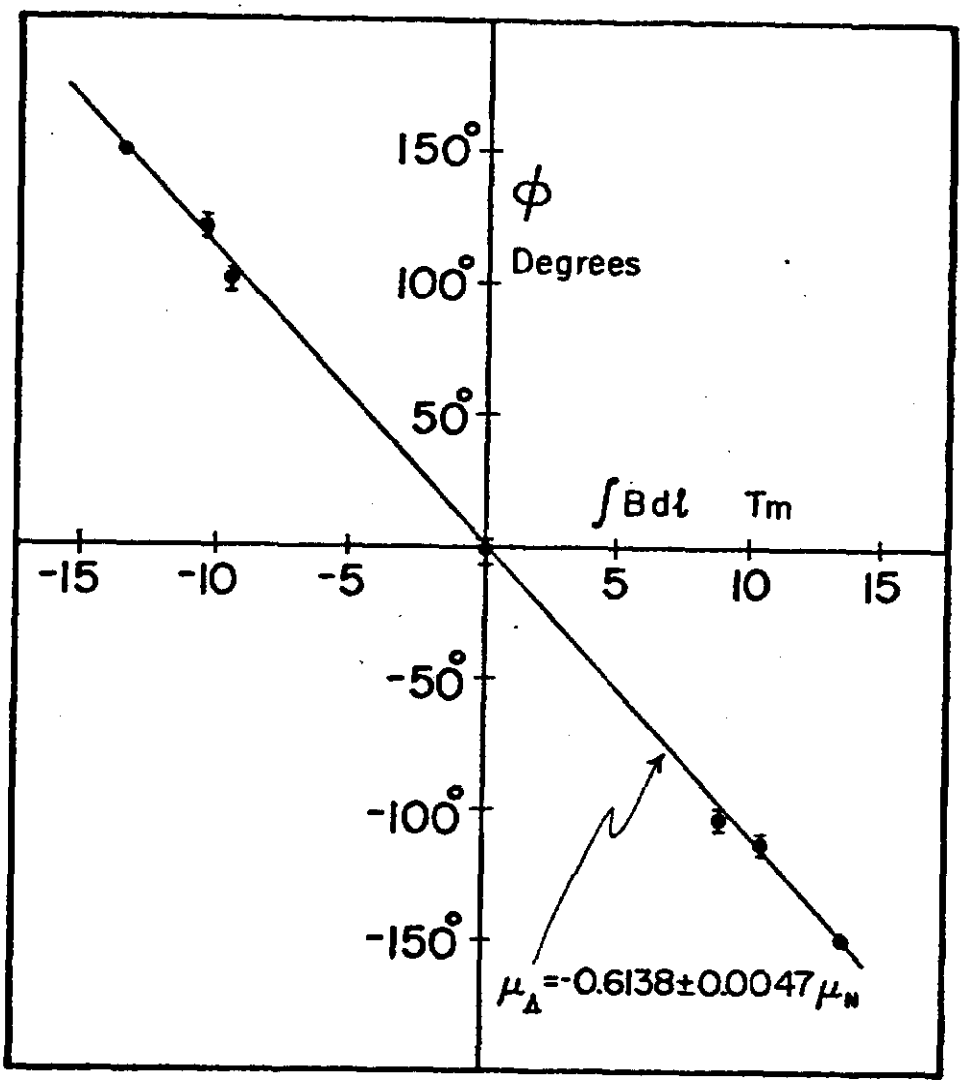
150°
φ
Degrees
100°
50°
∫ B dl Tm
-15
-10
-5
5
10
15
-50°
-100°
-150°
μΛ=-0.6138±0.0047 μN

Fig. 12

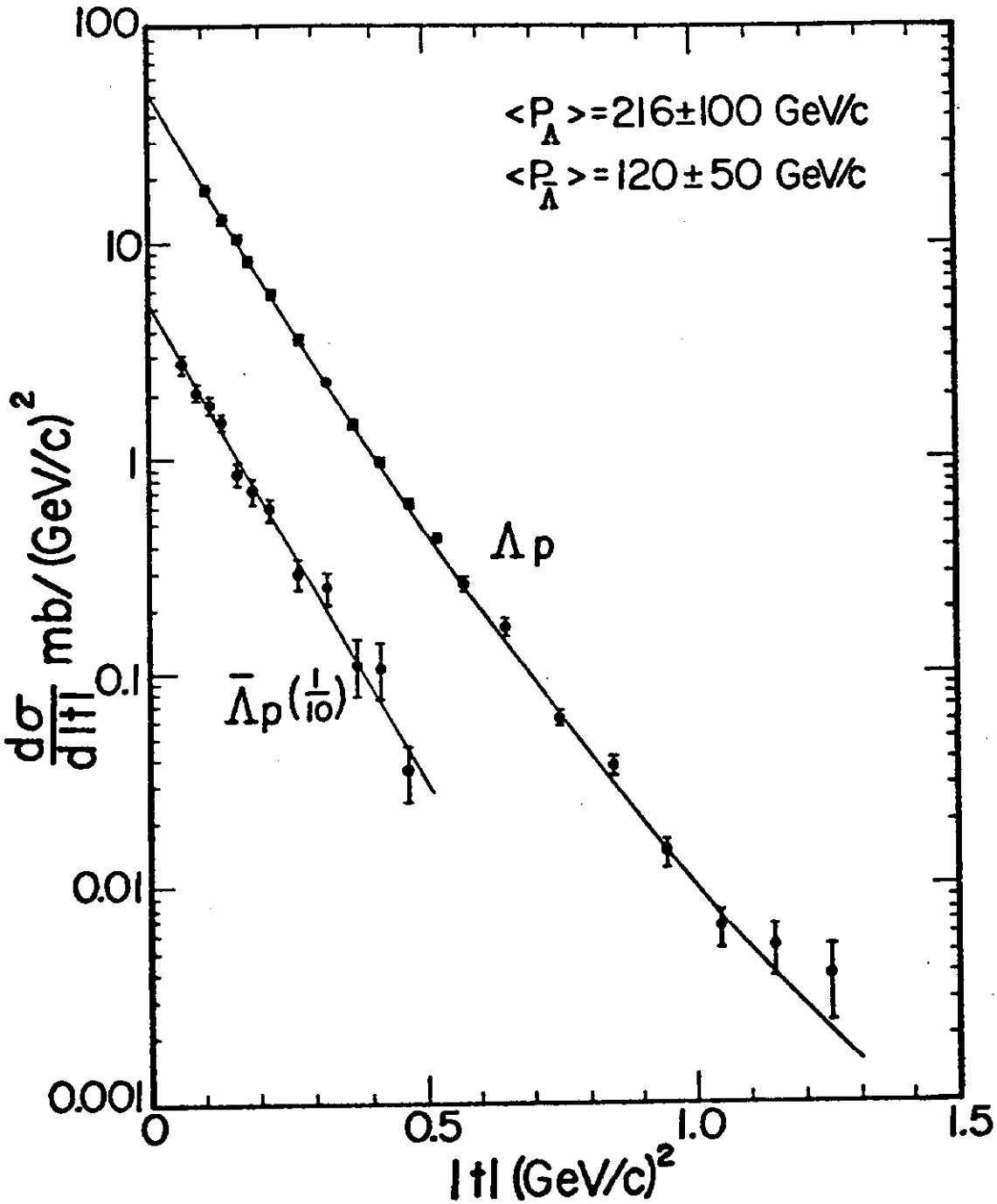
100
10
1
0.1
0.01
0.001
0
0.5
1.0
1.5
$\frac{d\sigma}{d|t|}$ mb/(GeV/c)^2
$|t|$ (GeV/c)^2
<P_Λ> = 216±100 GeV/c
<$P_{\bar{\Lambda}}$> = 120±50 GeV/c
Λp
$\bar{\Lambda} p$ ($\frac{1}{10}$)

Fig. 13

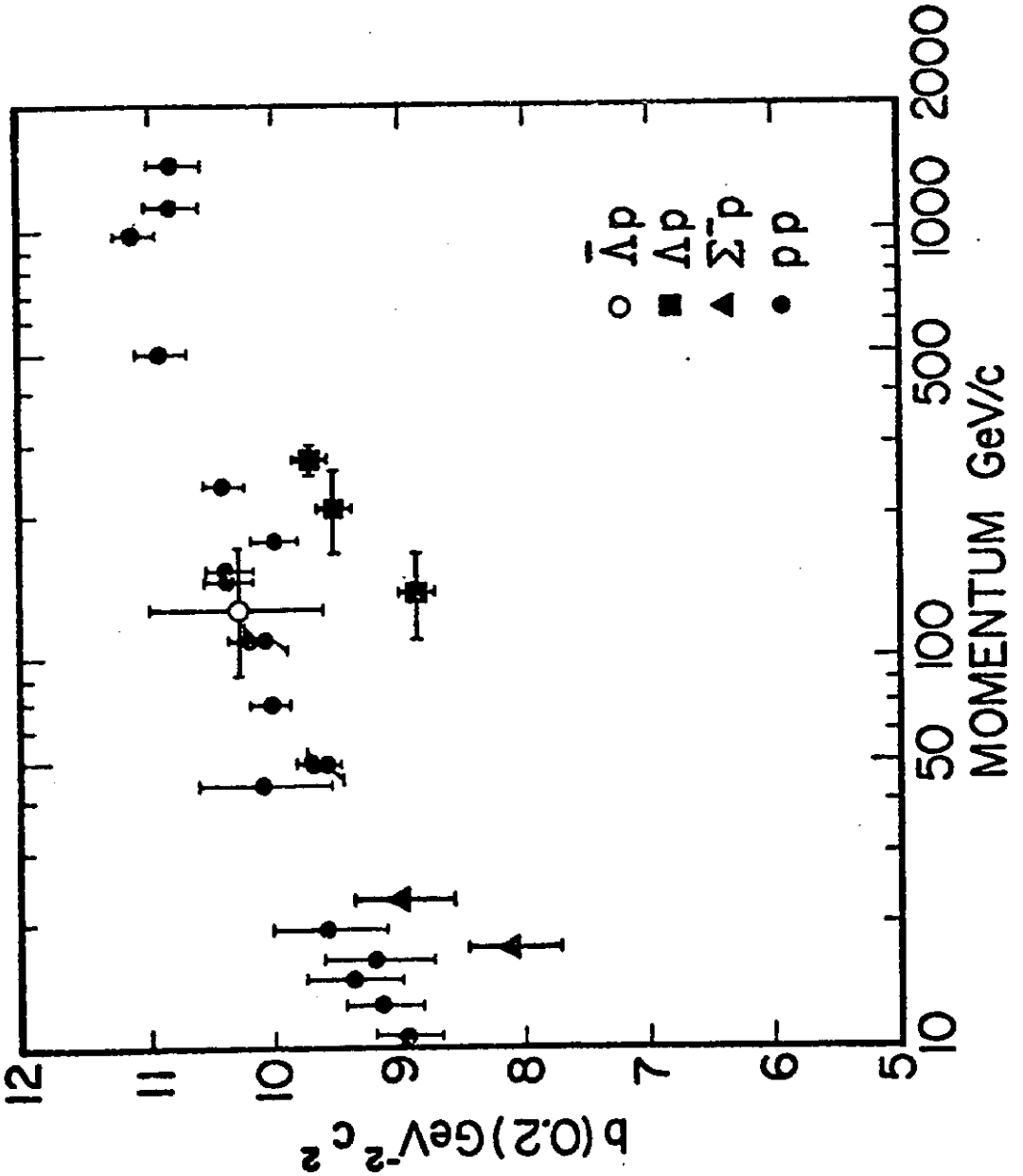
b (0.2) GeV⁻² c²
12
11
10
9
8
7
6
5
10
50
100
500
1000
2000
MOMENTUM GeV/c
p p
Σ⁻ p̄
Λ p̄
Λ̄ p̄

Fig. 14

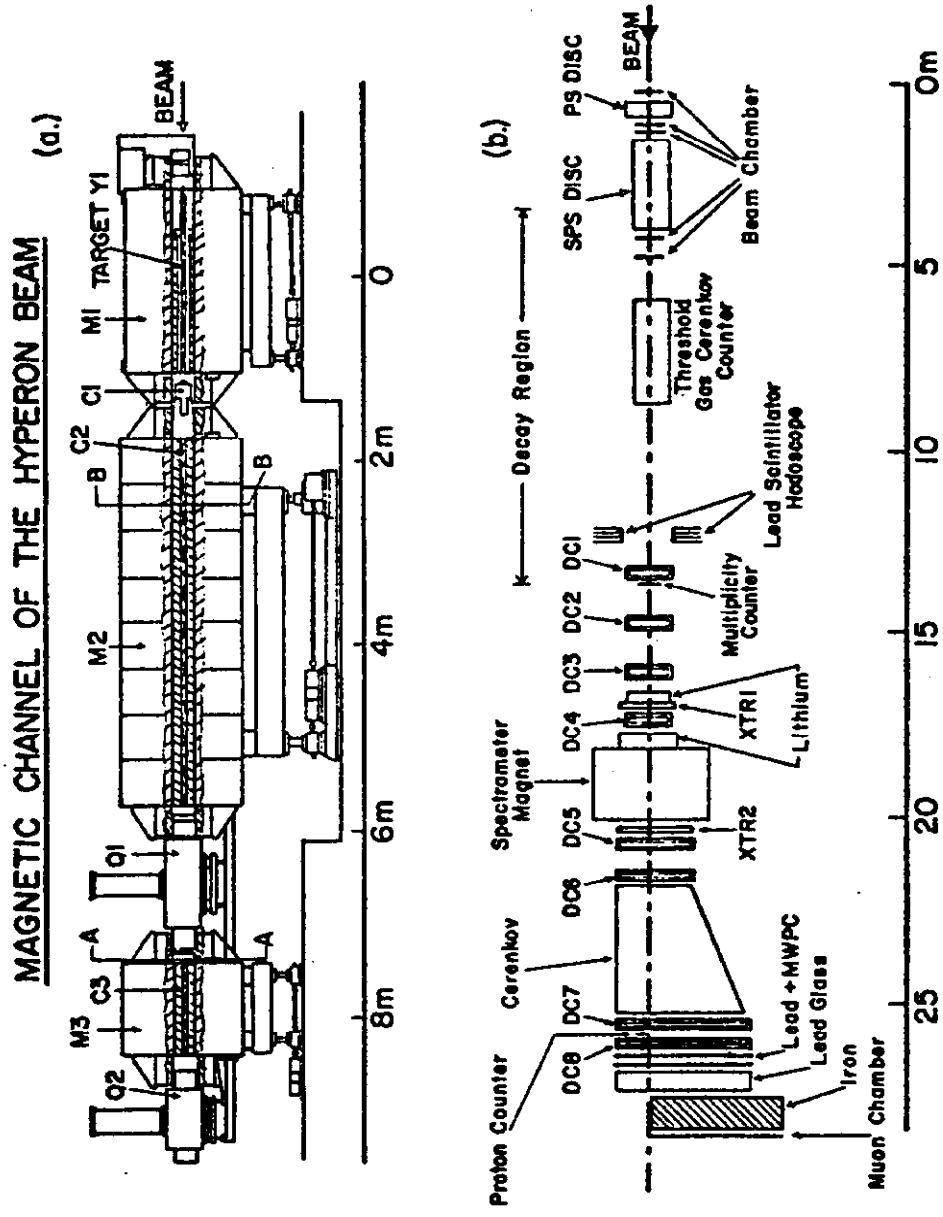
MAGNETIC CHANNEL OF THE HYPERON BEAM
(a.)
BEAM
TARGET Y1
M1
C1
C2
B
M2
Q1
A
C3
M3
Q2
0
2m
4m
6m
8m
(b.)
Decay Region
PS DISC
SPS DISC
BEAM
Beam Chamber
Threshold Gas Cerenkov Counter
Lead Scintillator Hodoscope
DC1
DC2
Multiplicity Counter
DC3
DC4
XTR1
Lithium
Spectrometer Magnet
DC5
XTR2
DC6
Cerenkov
DC7
DC8
Proton Counter
Lead + MWPC
Lead Glass
Iron
Muon Chamber
0m
5
10
15
20
25

Fig. 15

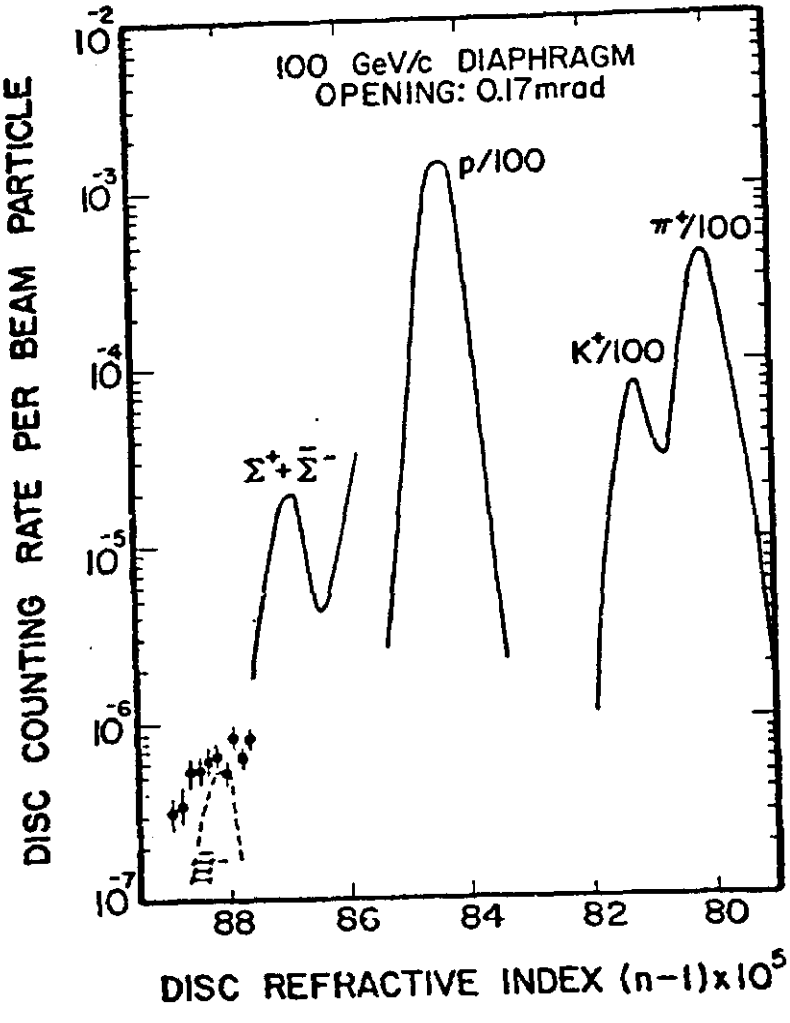
100 GeV/c DIAPHRAGM
OPENING: 0.17mrad
p/100
π⁺/100
K⁺/100
Σ⁺+Σ⁻
Ξ⁻
DISC COUNTING RATE PER BEAM PARTICLE
DISC REFRACTIVE INDEX (n-1)x10⁵
10⁻²
10⁻³
10⁻⁴
10⁻⁵
10⁻⁶
10⁻⁷
88
86
84
82
80

Fig. 16

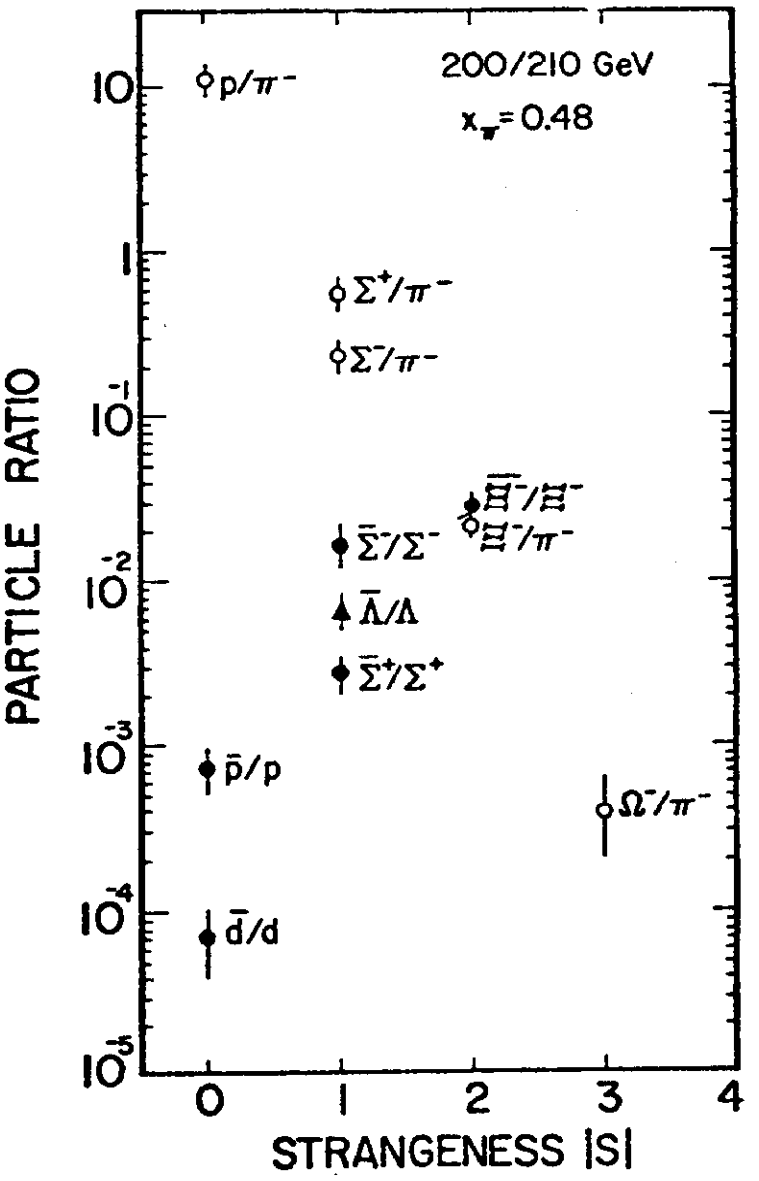
200/210 GeV
$x_\pi = 0.48$
p/π^-
Σ^+/π^-
Σ^-/π^-
$\bar{\Xi}^-/\Xi^-$
Ξ^-/π^-
$\bar{\Sigma}^-/\Sigma^-$
$\bar{\Lambda}/\Lambda$
$\bar{\Sigma}^+/\Sigma^+$
$\bar{p}/p$
Ω^-/π^-
$\bar{d}/d$
PARTICLE RATIO
STRANGENESS |S|

Fig. 17

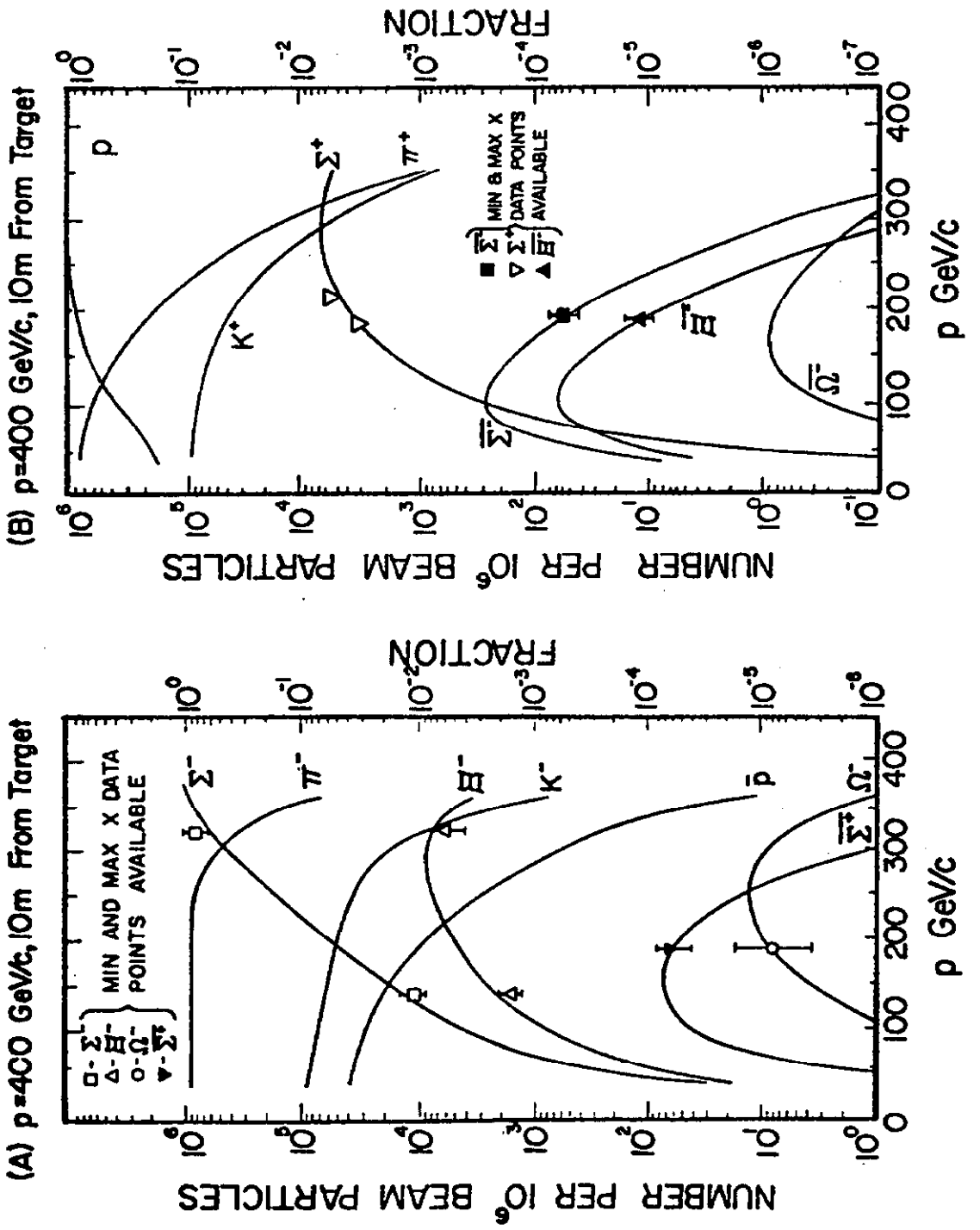
(A) p=400 GeV/c, 10m From Target
NUMBER PER 10^6 BEAM PARTICLES
FRACTION
p GeV/c
MIN AND MAX X DATA POINTS AVAILABLE
Σ^-
π^-
Ξ^-
K^-
$\bar{p}$
Ω^-
$\bar{\Sigma}^-$
(B) p=400 GeV/c, 10m From Target
NUMBER PER 10^6 BEAM PARTICLES
FRACTION
p GeV/c
MIN & MAX X DATA POINTS AVAILABLE
p
K^+
Σ^+
π^+
$\bar{\Sigma}^-$
$\bar{\Xi}^+$
$\bar{\Omega}^-$

Fig. 18